

# Twisted (co)homology of non-orientable Weyl semimetals

Thijs Douwes<sup>1</sup> and Marcus Stålhammar<sup>1,2\*</sup>

<sup>1</sup> Institute of Theoretical Physics, Utrecht University  
Princetonplein 5, 3584CC Utrecht, The Netherlands

<sup>2</sup> Department of Physics and Astronomy  
Uppsala University, Uppsala, Sweden

\* [marcus.backlund@physics.uu.se](mailto:marcus.backlund@physics.uu.se)

## Abstract

The quasi-particle excitations in Weyl semimetals, known as Weyl fermions, are usually forced to emerge in charge-conjugate pairs by the Nielsen–Ninomiya theorem. When the Brillouin zone is non-orientable, this constraint is replaced by a  $\mathbb{Z}_2$  charge cancellation, as a result of the chirality becoming ill-defined on such manifolds; this results in configurations with seemingly non-zero total chirality. Here, we set out to explain this behaviour from a purely topological perspective, and provide a classification of non-orientable Weyl semimetal topology in terms of exact sequences of twisted (co)homology groups. This leads to several discoveries of direct physical importance: in particular, we recover the  $\mathbb{Z}_2$  charge cancellation in a coordinate-independent way, allowing meaningful limits to be set on its physical interpretation. A detailed discussion is provided on a specific Klein bottle-like topology induced by a momentum-space glide symmetry, including a full review of the insulating and semimetallic invariants of the system and a classification of the surface states on the non-orientable boundary. Beyond this, we provide a complete survey of all possible non-orientable Brillouin zones and their associated invariants, and extend our formalism into the realm of non-Hermitian topological physics and inversion-symmetric Weyl semimetals. Our work exemplifies the vast potential of fundamental mathematical descriptions to not only aid the corresponding physical intuition, but also predict novel and hitherto overlooked phenomena of great relevance throughout the physics research forefront.

## Contents

<b>1</b>	<b>Introduction</b>	<b>2</b>
<b>2</b>	<b>Background</b>	<b>4</b>
2.1	Weyl semimetal topology: a physicist's approach	4
2.2	Weyl semimetal topology: a cohomology approach	5
2.3	Weyl semimetal topology: a homology approach	7
2.4	Bulk–boundary correspondence via homology	9
2.5	Non-orientable systems	10
<b>3</b>	<b>Non-orientable (co)homology formalism</b>	<b>11</b>
<b>4</b>	<b>Topology of <math>K^2 \times S^1</math></b>	<b>14</b>
4.1	Mod 2 charge cancellation	15

4.2	Topological invariants	15
4.3	$K^2$ surface states	18
<b>5</b>	<b>Extensions</b>	<b>19</b>
5.1	Additional non-orientable Brillouin zones	19
5.2	Non-Hermitian systems	22
5.3	Inversion symmetry	23
<b>6</b>	<b>Summary, discussion and outlook</b>	<b>27</b>
6.1	Summary	27
6.2	Discussion and outlook	28
<b>7</b>	<b>Conclusion</b>	<b>30</b>
	<b>References</b>	<b>31</b>

---

## 1 Introduction

The fusion of the mathematical framework of topology and condensed matter physics has revolutionised the understanding of quantum matter during the past decades. Following the hallmark discovery of the quantum Hall effect in the 1980s [1], a prominent advancement was realised in the classification of Bloch bands [2], paving the way towards a more rigorous understanding of the topological phases of matter. These phases include gapped insulators and superconductors [3, 4], as well as gapless semimetals such as graphene [5] and Weyl semimetals [6, 7]. The latter are three-dimensional materials hosting so-called Weyl points or Weyl nodes, where the valence and conduction bands coincide. These band crossing points are considered accidental, in the sense that they are not enforced by any symmetry of the system. They are, however, topological in nature, which ensures that they are robust to external perturbations; for example, a Weyl semimetal may be subjected to some disorder without removing the Weyl nodes. Weyl semimetals find profound applications not only in material science [8–10], where their transport properties suggest technical applications in future solar cells [11–13], but also in particle physics, allowing Weyl fermions to be studied as quasi-particle excitations [14], in photonic crystals [15], and in constructing laboratory setups which potentially mimic features in analogue quantum gravity such as black holes [16–22].

From a physical point of view, the topological properties of Weyl nodes are usually thought of in terms of quasiparticle charges: each Weyl node can be assigned an integer monopole charge describing the flux of a gauge field around the corresponding quasiparticle [6, 7]. These charges are explicitly chiral in nature, relating to the chirality of the corresponding Weyl fermion quasiparticles. In periodic structures, where the Brillouin zone takes the form of a three-dimensional torus, the total charge is constrained to vanish, forbidding any non-zero net gauge flux [23–33]. This constraint is known as the Nielsen–Ninomiya theorem, and it effectively forces the Weyl nodes to emerge in pairs [34–36], with each node being associated with a partner of opposite chirality. Upon merging within the Brillouin zone, positive and negative Weyl nodes may annihilate in pairs, leaving a gapped band structure.

Mathematically, these features can be formally described using the theory of characteristic classes and the language of homology and cohomology [37, 38]. Studies have shown that relatively simple arguments involving a so-called Mayer–Vietoris sequence of cohomology groups

can provide a deeper understanding of the structure and origin of these topological features of Weyl semimetals. For example, the Nielsen–Ninomiya theorem follows directly from the exactness of this sequence; the well-established Poincaré duality between homology and cohomology groups generates an interpretation of Weyl point topology in terms of *Dirac strings* (strings of gauge singularities between the Weyl nodes); the celebrated bulk–boundary correspondence is formalised by letting the surface projection act on homology groups, providing mathematical context to surface Fermi arcs as projections of these Dirac strings; and finally, the entries of the (co)homology groups classify the possible topological invariants, corresponding precisely to topologically distinct Berry curvatures. The (co)homology groups can hence be used to obtain a relatively straightforward, yet formally correct, understanding of the global and local topology of Weyl semimetals, without relying on far more involved classifications based on K-theory [39–46].

Although Weyl nodes arise independently of additional symmetries, the presence of such symmetries may in fact alter their topological properties, and hence their (co)homology description. An experimentally significant example of this is the impact of time reversal symmetry. To account for this symmetry, the authors of Ref. [47] show that the (co)homology sequences, as well as the conventional Poincaré duality, need to be modified. The correct classification is then performed using so-called equivariant homology and twisted equivariant cohomology groups [47, 48], and includes a complete description of all (weak and strong) invariants for gapped (insulating) as well as gapless (semimetallic) phases. The presence of time reversal symmetry effectively halves the Brillouin zone into *fundamental domains*; all physical properties of momenta in one half are mirrored to the other half, with the exception of the eight time-reversal invariant momenta; the presence of these special momenta prevents the fundamental domain from being considered a Brillouin zone in its own right.

Recently, a class of non-symmorphic (i.e. combining rotation/reflection with fractional lattice translations) momentum-space symmetries that lack such fixed momenta has been studied, leading to fundamentally altered Brillouin zone topologies. Of particular interest in this work are the orientation-reversing symmetries, under which the fundamental domain becomes non-orientable [49–53]. This loss of orientability causes the chirality of Weyl nodes to become ill defined; this has recently been used to study setups where the constraints imposed by the Nielsen–Ninomiya theorem are circumvented. Concretely, the authors of Ref. [49] show that Weyl nodes emerging in non-orientable Brillouin zones are not necessarily charge-conjugate to each other: a Weyl node with topological invariant  $\pm 1$  is no longer always accompanied by a partner with topological invariant  $\mp 1$ ; instead, the partner may have the same topological invariant. In general terms, the authors derive a mod 2 charge cancellation theorem, rather than the conventional complete charge cancellation imposed by the Nielsen–Ninomiya theorem.

Although the work in Ref. [49] is of indisputable importance, highlighting the vital role that the topology of the Brillouin zone plays in Weyl semimetal topology, the arguments given have a crucial limitation: the definition of the topological invariants depends on a particular choice of a fundamental domain, which amounts to a choice of orientation upon integration. This ambiguity highlights the imminent need for a coordinate-free topological description, independent of any particular fundamental domain. We develop such a description in this work, applicable to systems in which non-orientable fundamental domains are induced by symmetries, and use the particular system studied in Ref. [49] as an illustrative example. We modify the aforementioned classification scheme in terms of (co)homology groups, showing that the homology groups must be twisted in order to account for the loss of orientability under this specific symmetry. The use of these twisted homology groups gives rise to the concepts of *twisted Dirac strings* and *twisted Fermi arcs*, which can be used to great effect to gain intuition for the underlying topological invariants and their physical interpretation. We also directly verify the mod 2 charge cancellation found in Ref. [49], now within a mathematically rigorous

and coordinate-free context. In addition, we discuss an emergent  $\mathbb{Z}$  invariant associated with this specific system.

To illustrate the utility of this more abstract classification scheme, we further investigate all other non-symmorphic momentum-space symmetries which give rise to non-orientable Brillouin zones, providing the associated groups of invariants in each case. We also show how this description can be applied to non-Hermitian systems to describe the topology of exceptional points (non-Hermitian degeneracies where not only the energy bands but also the associated eigenstates coalesce) in non-orientable fundamental domains, formalising the two-band case of the very recent works in Refs. [54, 55]. Lastly, we also provide heuristic arguments addressing the highly relevant case of inversion-symmetric Weyl semimetals within this framework, further exemplifying its usefulness and relevance. Our work thus provides a fundamental mathematical understanding of the topology of gapped and gapless systems with non-orientable fundamental domains, straightens out the physical interpretation and the topological origin of the corresponding invariants without resorting to more abstract K-theory arguments, and paves the way towards a deeper and more physically direct mathematical understanding of the impact of symmetries in topological band theory.

The remainder of this work is organised as follows: we begin in Sec. 2 by providing the necessary theoretical background on Weyl semimetal topology, comparing the conventional physical approach with the (co)homology approach. We also offer a brief overview of the way in which non-orientable Brillouin zones arise, especially as it pertains to Weyl semimetals. In Sec. 3 we comment on some fundamental ambiguities in the current description of non-orientable Weyl semimetals, serving as a motivation for extending the coordinate-free (co)homology description into the non-orientable regime. We then perform this extension by arguing how the (co)homology descriptions should be altered under orientation-reversing symmetries. We apply these findings in Sec. 4 to provide a concrete classification of three-dimensional Weyl semimetals subject to a momentum-space glide symmetry. Section 5 revolves around several additional applications of this classification scheme, focussing on additional non-orientable Brillouin zones, non-Hermitian systems, and inversion-symmetric Weyl semimetals. Our results are summarised and contextualised in Sec. 6, where we clarify important physical consequences and suggest avenues for future research. We take stock and conclude in Sec. 7.

## 2 Background

We devote this section to a brief background on two topics that are central to this work: coordinate-free descriptions of the topological features of Weyl semimetals (Secs. 2.2, 2.3 and 2.4), and the emergence of non-orientable Brillouin zones (Sec. 2.5). A more conventional discussion (from the point of view of a physicist) on Weyl semimetal topology is given in Sec. 2.1, allowing for a comparison between the physical and mathematical pictures. Readers who are familiar with these topics may proceed to Sec. 3, although it should be noted that the notation and other semantics introduced in this section will be used throughout the rest of the manuscript.

### 2.1 Weyl semimetal topology: a physicist's approach

A generic two-band system may be described by a Bloch Hamiltonian, the most general form of which takes the form

$$\mathcal{H}(\mathbf{k}) = d_0(\mathbf{k})\sigma^0 + \mathbf{d}(\mathbf{k}) \cdot \boldsymbol{\sigma}, \quad (1)$$

where  $\sigma^0$  denotes the  $2 \times 2$  identity matrix,  $\boldsymbol{\sigma} = (\sigma^x, \sigma^y, \sigma^z)$  is the vector of Pauli matrices,  $\mathbf{k}$  the lattice momentum,  $d_0 : \mathbb{T}^d \rightarrow \mathbb{R}$ , and  $\mathbf{d} : \mathbb{T}^d \rightarrow \mathbb{R}^3$ . The energy bands of the system then correspond to the two eigenvalues of this Hamiltonian, which are given by

$$E_{\pm}(\mathbf{k}) = d_0(\mathbf{k}) \pm |\mathbf{d}(\mathbf{k})| := d_0(\mathbf{k}) \pm \sqrt{\mathbf{d}(\mathbf{k}) \cdot \mathbf{d}(\mathbf{k})}. \quad (2)$$

The two bands touch when these eigenvalues are degenerate, which happens precisely when  $\mathbf{d}(\mathbf{k}) = 0$ . In a  $d$ -dimensional system, this amounts to solving a system of three equations with  $d$  parameters. For  $d \geq 3$ , such systems may have generic solutions that do not depend on external symmetries; these solutions result in so-called *accidental band crossings* [6]. In three dimensions, these crossings tend to occur at isolated momenta called *Weyl points* or *Weyl nodes*, whose name stems from the fact that, to first order, the Hamiltonian at such a point resembles that of a chiral Weyl fermion. These points are topological in nature, which means that they are stable under any sufficiently small perturbation, including (but not limited to) physical disorder. The topology of a Weyl point is characterised by an integer invariant, related to the chirality of the corresponding Weyl fermion. This invariant can be computed as the flux of the Berry field through a sphere enclosing each point:

$$\chi = \frac{1}{2\pi} \oint_{S^2} \mathcal{F} \in \mathbb{Z}, \quad (3)$$

where  $\mathcal{F} = d\mathcal{A}$  is the field strength of the Berry potential  $\mathcal{A} = -i \langle \psi | d\psi \rangle$  over the occupied bands. In crystalline materials, the charges related to all Weyl nodes necessarily add up to zero across the Brillouin torus  $\mathbb{T}^3$ , which can be seen from a Stokes' theorem argument;

$$\sum_{i=1}^k \chi_i = \frac{1}{2\pi} \sum_{i=1}^k \oint_{S_i^2} \mathcal{F} = \frac{1}{2\pi} \int_{\mathbb{T}^3 \setminus W} d\mathcal{F} = 0, \quad (4)$$

where  $W = \{w_1, \dots, w_k\}$  denotes the discrete set of Weyl points. The last equality holds due to the Bianchi identity, which implies that the Berry field is divergence free. This cancellation of charges is often referred to as the Nielsen–Ninomiya theorem [34–36].

As is the case in topologically insulating materials, a bulk–boundary correspondence exists for Weyl semimetals: their bulk topology is reflected onto their surface, in the form of so-called *Fermi arcs*. These dispersionless surface states define curves on the two-dimensional surface Brillouin zones in momentum space, bounded by the surface projection of the Weyl points; see Fig. 1(a). These can be thought of as projections of the Fermi energy of two-dimensional gapped planes perpendicular to the surface, located between the Weyl points.

## 2.2 Weyl semimetal topology: a cohomology approach

We now change perspective to a more mathematical treatment of the features described above. Note that the description provided in the next few sections assumes that no additional symmetries beyond lattice translation are enforced on the system; it will become clear in Sec. 2.5 that some aspects of the formalism require modification later on.

From a differential geometry point of view, the Berry potential  $\mathcal{A}$  can be considered a connection 1-form, and the corresponding field strength  $\mathcal{F}$  is its curvature 2-form. Such curvature forms are classified topologically by a *second cohomology group*; in general, an  $n$ -th cohomology group  $H^n(M)$  on a manifold  $M$  roughly classifies obstructions for closed  $n$ -forms  $\omega$  on  $M$  (i.e. those with  $d\omega = 0$ ) to be exact (i.e. having the form  $\omega = d\eta$  for some  $(n-1)$ -form  $\eta$ ) [56]. These groups may be calculated and studied abstractly, without reference to specific differential forms such as the Berry curvature; this ensures that a great deal of topological information can be extracted from highly tractable calculations [57]. The elements of this

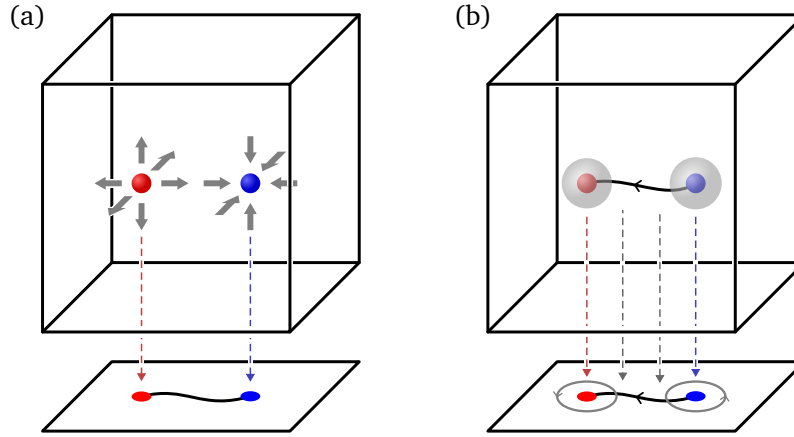


Figure 1: A schematic comparison between (a) the conventional physical interpretation of Weyl point topology and (b) the corresponding (co)homology picture. In (a), a positively (negatively) charged Weyl point is depicted as a source (sink) of the Berry field inside the Brillouin zone. After projection to a surface, these nodes form the endpoints of a physical Fermi arc. In the cohomology picture (b), the charges correspond to second cohomology classes on spheres surrounding the Weyl points. The oriented Dirac string connecting the two nodes represents a first homology counterpart to this: by Poincaré duality, the signed intersections of this string with the spheres agree with the cohomological charges. The Dirac string projects naturally onto a first homology class on the surface, which manifests as an oriented Fermi arc. Poincaré duality then ensures that the surface projections of the Weyl nodes have charges in terms of first cohomology classes on circles surrounding them.

abstract second cohomology group are called *second cohomology classes*, and they represent different topological phases of the system under consideration. In three dimensions, these second cohomology classes may be characterised completely by the *first Chern numbers* they induce on two-dimensional subspaces; the charge calculated on a 2-sphere in Eq. (3) is an example of one such first Chern number.

Since the Berry curvature has a singularity at each Weyl point, the corresponding topology is classified by curvatures away from these points; as a result, the topology of Weyl semimetals is classified by second cohomology on the punctured space  $\mathbb{T}^3 \setminus W$ , i.e. the Brillouin zone  $\mathbb{T}^3$  with the collection of Weyl points  $W$  removed. In particular, a three-dimensional Chern insulator can be considered a special case of a Weyl semimetal with zero Weyl points; as a result, its topology is classified by the second cohomology group of the full (unpunctured) torus  $\mathbb{T}^3$ .

The physical information contained in these groups is extracted using a *Mayer–Vietoris sequence*, a widely used tool within algebraic topology relating the cohomology of a space to that of a choice of subspaces [57]. By making the appropriate choice of subspaces, these sequences relate the topological charge of each individual Weyl point to the global Weyl semimetal topology [37, 38]. The common choice of subspaces covers the 3-torus as follows:

$$\mathbb{T}^3 = (\mathbb{T}^3 \setminus W) \cup \coprod_{i=1}^k D_i^3, \quad (5)$$

i.e. the Brillouin torus  $\mathbb{T}^3$  is covered by the punctured torus  $\mathbb{T}^3 \setminus W$  with the Weyl points removed, and a disjoint union of solid balls (3-discs)  $D_i^3$  centred on the respective Weyl points.



The relevant part of the corresponding Mayer–Vietoris sequence then reads

$$0 \rightarrow \underbrace{H^2(\mathbb{T}^3)}_{\text{3D Chern insulator}} \rightarrow \underbrace{H^2(\mathbb{T}^3 \setminus W)}_{\text{Semimetal}} \xrightarrow{\beta} \underbrace{\bigoplus_{w_i \in W} H^2(S_{w_i}^2)}_{\text{Local charges}} \xrightarrow{\Sigma} \underbrace{H^3(\mathbb{T}^3)}_{\text{Total charge}} \rightarrow 0. \quad (6)$$

Before moving on, let us comment on the physical meaning of each group individually. Starting on the left,  $H^2(\mathbb{T}^3)$  is exactly what provides the topology of a three-dimensional Chern insulator, which is given by a vector of three distinct Chern numbers  $\mathbf{C} = (C_x, C_y, C_z)$  [58]. These Chern numbers are calculated as Berry curvature integrals on two-dimensional toroidal slices of the Brillouin zone, similar to the Weyl point charge in Eq. (3):

$$C_i = \frac{1}{2\pi} \oint_{\mathbb{T}^2_{k_i=\text{const.}}} \mathcal{F} \in \mathbb{Z}, \quad (7)$$

where the integration domain is any slice of constant  $k_i$ . Second, the group  $H^2(\mathbb{T}^3 \setminus W)$  classifies all possible semimetallic phases given a fixed set of Weyl points  $W$ . Third, the collection of  $H^2(S_{w_i}^2)$  gives information about the local charges of each Weyl point  $w_i \in W$ . Finally, the third cohomology group  $H^3(\mathbb{T}^3)$  can be thought of as classifying total charge on the Brillouin torus, with the map  $\Sigma$  acting as a sum over the individual charges; as a result, non-zero elements of this group represent unphysical configurations.

The groups in Eq. 6 can be calculated explicitly, after which the sequence takes the form

$$0 \rightarrow \mathbb{Z}^3 \rightarrow \mathbb{Z}^3 \oplus \mathbb{Z}^{k-1} \xrightarrow{\beta} \mathbb{Z}^k \xrightarrow{\Sigma} \mathbb{Z} \rightarrow 0, \quad (8)$$

where  $k = |W|$  is the number of Weyl points in the system. The relation between local and global topological properties is provided by the maps between these groups. These maps are not independent of each other; Mayer–Vietoris sequences are known to be *exact*, meaning that the image of one map is always equal to the kernel of the next map in the sequence. This exactness sets restrictions on the way in which the elements of each group are mapped into the subsequent one.

There are two features of this sequence that are of particular interest from the perspective of semimetal topology. The first of these relates to the maps  $\beta$  and  $\Sigma$  around the group of local charges  $\mathbb{Z}^k$  in Eq. 8; here, exactness implies that  $\text{im}(\beta) = \ker(\Sigma)$ . That is, the local Chern numbers sum to zero if and only if they descend from a semimetal structure. This tells us two different things: the first is that the sum of Weyl point chiralities in a Weyl semimetal is necessarily zero; this is precisely the content of the Nielsen–Ninomiya theorem. In addition, it also implies the converse: any configuration of charges that sums to zero is necessarily compatible with global semimetal topology.

The second important feature of this sequence lies in the nature of the semimetal group  $H^2(\mathbb{T}^3 \setminus W)$  itself. Its appearance between a group of insulating invariants and the charge cancellation construction discussed above signifies that semimetal topology can be fundamentally understood as a product of these two aspects. This is precisely the reason for the suggestive notation  $\mathbb{Z}^3 \oplus \mathbb{Z}^{k-1}$  of this group: for any given set of  $k$  Weyl points there are  $\mathbb{Z}^{k-1}$  valid charge configurations (i.e.  $k$  different  $\mathbb{Z}$ -valued charges subject to one  $0 \in \mathbb{Z}$  charge cancellation constraint), and for any such configuration, the topology is further determined by a  $\mathbb{Z}^3$  background of insulating invariants of the form of the Chern numbers  $C_i$  of Eq. (7).

### 2.3 Weyl semimetal topology: a homology approach

The theory of cohomology has a natural dual in homology: the  $n$ -th homology group  $H_n(M)$  (note the lowered index  $n$ ) describes classes of  $n$ -dimensional closed oriented subspaces of a

manifold  $M$ . In physical terms, these are precisely the subspaces on which the integration of the  $n$ -forms classified by cohomology yields consistent values: for example, the 2-sphere  $S^2$  on which the Berry curvature integral is evaluated in Eq. (3) represents a second homology class on the punctured torus.

This natural duality between cohomology and homology is not precise enough to carry the classification of topological phases over to the homology setting. However, there is a more precise statement called *Poincaré duality* that does allow for a homology classification: it states that for a closed oriented  $d$ -dimensional manifold  $M$ , the following isomorphism holds for any integer  $n$ :

$$H_n(M) \cong H^{d-n}(M). \quad (9)$$

This duality allows the second cohomology groups involved in classifying invariants to be reframed as first homology groups: that is, there is a classification based on one-dimensional subspaces of the Brillouin zone. The semimetal Mayer–Vietoris sequence in Eq. (6) dualises to the following form:

$$0 \rightarrow \underbrace{H_1(\mathbb{T}^3)}_{\text{Dirac loops}} \rightarrow \underbrace{H_1(\mathbb{T}^3, W)}_{\text{Dirac strings}} \xrightarrow{\partial} \underbrace{H_0(W)}_{\text{Local charges}} \xrightarrow{\Sigma} \underbrace{H_0(\mathbb{T}^3)}_{\text{Total charge}} \rightarrow 0. \quad (10)$$

Note that this is a valid exact sequence in homology independently of the validity of Poincaré duality in a given setting; the duality only ensures that it classifies the same topology as the cohomology sequence.

Special attention should be paid to the second group in this sequence, which is the dual of the semimetal invariant group  $H^2(\mathbb{T}^3 \setminus W)$  on the punctured torus; since  $\mathbb{T}^3 \setminus W$  is not a closed space, a slightly modified argument (based on *Lefschetz duality*) gives rise to the *relative* homology group  $H_1(\mathbb{T}^3, W)$  with respect to the set of Weyl points  $W$ . The result is that the oriented one-dimensional spaces it classifies are allowed to terminate at the Weyl points; an example of this is shown in Fig. 1(b). Such spaces are called *Dirac strings*, in reference to the fact that they can be physically considered to be strings of gauge singularities running between Weyl nodes.

Positively charged Weyl nodes are always connected by a Dirac string to a negatively charged one, and vice versa. As a result of this, the Nielsen–Ninomiya theorem is encoded in the homology sequence in Eq. (10) in a very natural way: the boundary map  $\partial$  assigns opposite charges to the Weyl nodes at opposite ends of a Dirac string, and these sum to zero by nature when the map  $\Sigma$  is applied.

The first group in the sequence classifies the insulating topology in terms of what we will refer to as *Dirac loops*. These can be thought of as Dirac strings which are closed into loops along the periodic directions of the torus, and indeed such loops may form when Weyl nodes are annihilated together along topologically non-trivial paths. In this regard, Weyl semimetals can be considered transitional phases between different insulating topological phases; this is precisely why a group of insulating invariants appears in each of the exact sequences under consideration.

Finally, the Poincaré duality that relates the homology and cohomology classifications has a natural geometric consequence in any given topological phase: for any two-dimensional surface within the Brillouin zone, the (cohomological) Chern number on that surface agrees with the number of signed intersections it has with (homological) oriented Dirac strings or loops. For example, a Dirac loop that spans  $\mathbb{T}^3$  once in the  $k_x$ -direction precisely induces a unit Chern number  $C_x$ , as defined in Eq. (7). Similarly, the orientation of a Dirac string always agrees with the cohomological charge of the Weyl nodes at either end, defined on the 2-spheres surrounding them – this is also illustrated in Fig. 1(b). Seeing as Poincaré duality depends on orientability of the Brillouin zone, this is one of the aspects that needs to be treated carefully in the non-orientable case.



## 2.4 Bulk–boundary correspondence via homology

As noted in Sec. 2.1, the bulk topology of Weyl semimetals gives rise to surface Fermi arcs via the bulk–boundary correspondence. This correspondence can be made precise using the language of homology. To this end, assume the existence of a projection  $\pi : \mathbb{T}^3 \rightarrow \mathbb{T}^2$  that maps the bulk onto a two-dimensional surface Brillouin torus, and let  $W' := \pi(W)$  denote the surface projection of the set of Weyl nodes  $W$ . The projection  $\pi$  induces a map  $\pi_*$  between homology groups, called the *pushforward* on homology classes:

$$\pi_* : H_1(\mathbb{T}^3, W) \rightarrow H_1(\mathbb{T}^2, W'), \quad [s] \mapsto [\pi(s)], \quad (11)$$

where  $[s]$  denotes the homology class corresponding to a Dirac string configuration  $s$  (i.e. the set of Dirac strings which are topologically equivalent to  $s$ ). As it turns out, the resulting surface homology class  $\pi_*([s]) := [\pi(s)]$  is precisely the homology class of the physical Fermi arc [37, 38, 59]. In other words, loosely speaking, Fermi arcs can be considered surface projections of bulk Dirac strings; this is illustrated in Fig. 1(b).

One can apply similar reasoning to the rest of the exact sequence in Eq. (10), resulting in a similar exact sequence on the surface:

$$0 \rightarrow \underbrace{H_1(\mathbb{T}^2)}_{\text{Fermi loops}} \rightarrow \underbrace{H_1(\mathbb{T}^2, W')}_{\text{Fermi arcs}} \xrightarrow{\partial} \underbrace{H_0(W')}_{\text{Surface charges}} \xrightarrow{\Sigma} H_0(\mathbb{T}^2) \rightarrow 0. \quad (12)$$

Calculated in terms of explicit groups, this sequence takes on a similar form to Eq. (8):

$$0 \rightarrow \mathbb{Z}^2 \rightarrow \mathbb{Z}^2 \oplus \mathbb{Z}^{k-1} \xrightarrow{\partial} \mathbb{Z}^k \xrightarrow{\Sigma} \mathbb{Z} \rightarrow 0. \quad (13)$$

This sequence is in many ways analogous to its bulk counterpart; in particular, the boundary map  $\partial$  and the summation  $\Sigma$  retain the same interpretation, indicating that the Nielsen–Ninomiya theorem is also topologically enforced on the surface. The *Fermi loops* appearing in the leftmost group are boundary states of three-dimensional Chern insulators, which result from closing Fermi arcs into non-trivial loops – a process which has been observed experimentally [60].

Finally, the surface topology can also be framed in terms of cohomology, allowing for a more direct physical interpretation. This is achieved by another application of Poincaré duality, with the key difference that the first homology groups are dualised to *first* instead of second cohomology groups due to the two-dimensional nature of the surface Brillouin zone. The dual of the homology sequence in Eq. (12) is then equivalent to the following Mayer–Vietoris sequence:

$$\dots \xrightarrow{0} \underbrace{H^1(\mathbb{T}^2) \rightarrow H^1(\mathbb{T}^2 \setminus W')}_{\text{Gapless boundary states}} \rightarrow \underbrace{\bigoplus_{\tilde{w}_i \in W'} H^1(S_{\tilde{w}_i}^1)}_{\text{Surface charges}} \xrightarrow{\Sigma} H^2(\mathbb{T}^2) \rightarrow 0. \quad (14)$$

As a small note, the group to the left of this sequence is formally non-zero in the full Mayer–Vietoris sequence due to the low dimensionality, but since it maps trivially into  $H^1(\mathbb{T}^2)$ , the interpretation is unchanged.

Physically speaking, the appearance of first cohomology groups in this sequence implies that the surface invariants in these systems can be calculated by integration of 1-forms; for example, as illustrated in Fig. 1(b), the topological charge of a projected Weyl node  $\tilde{w}$  can be calculated as a winding number of the Berry phase on a small circle  $S_{\tilde{w}}^1$  enclosing it.

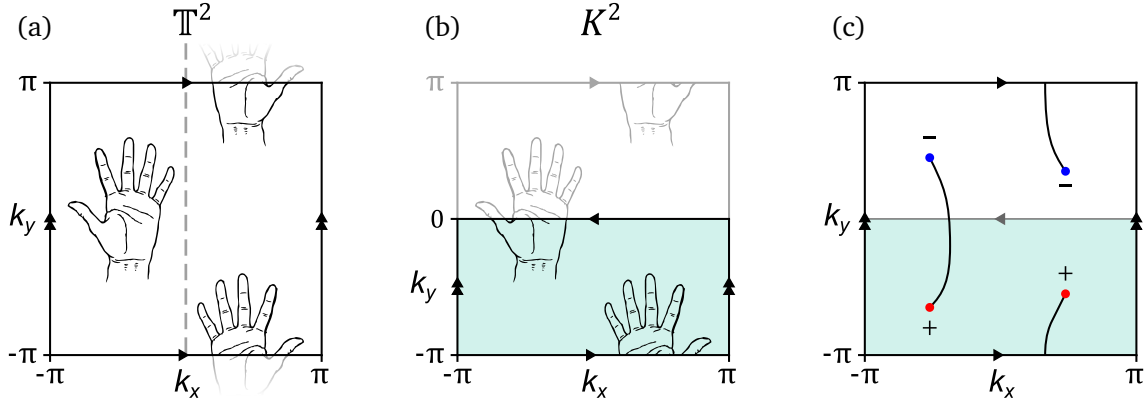


Figure 2: Illustration of the effect of glide symmetry on a two-dimensional Brillouin zone. (a) The symmetry acts on objects in the Brillouin zone by simultaneous reflection and translation, changing their handedness. On the full torus  $\mathbb{T}^2$ , the chiralities of the resulting objects are still well defined. (b) After reduction to the shaded fundamental domain, the Brillouin zone becomes non-orientable. The notion of handedness is lost in the process: the left palm traversing the orientation-reversing line at  $k_y = 0$  emerges as a right palm at  $k_y = -\pi$ . (c) Equivalent behaviour appears on the surface Brillouin zone of a glide symmetric Weyl semimetal: from the perspective of the shaded fundamental domain, a Fermi arc which crosses  $k_y = 0$  appears to connect similarly charged Weyl nodes.

## 2.5 Non-orientable systems

As noted earlier, exposing a system to various symmetries may drastically alter its topological properties. In this work, we are concerned with orientation-reversing symmetries, and in particular those which give rise to alternate Brillouin zone topologies. Such alternate Brillouin zones were first explored in two dimensions in Ref. [50], in which gauge fluxes on a real-space lattice give rise to a so-called *glide symmetry* in momentum space. This symmetry combines a reflection along the  $k_x$ -axis with a half-lattice translation along the  $k_y$ -axis; see Fig. 2(a). Explicitly, the momentum-space Hamiltonian is subject to the constraint

$$\mathcal{H}(k_x, k_y) = U\mathcal{H}(-k_x, k_y + \pi)U^{-1}. \quad (15)$$

A special property of this glide symmetry is that its action on the Brillouin torus  $\mathbb{T}^2$  is free, i.e. it leaves no points fixed. As a result, the physics of the system is completely captured on a *fundamental domain* covering precisely half of the torus with  $-\pi \leq k_y \leq 0$ , which thus acts as the new Brillouin zone. Under the correct boundary identifications, this fundamental domain takes on the topology of the non-orientable Klein bottle  $K^2$ ; see Fig. 2(b). In this specific instance, the loss of orientability changes the  $\mathbb{Z}$ -valued Chern number that would normally be expected in the system to an invariant valued in  $\mathbb{Z}_2 = \{0, 1\}$ ; that is, the system has only one trivial and one topological phase.

This concept has recently been applied in the three-dimensional setting of Weyl semimetals in Ref. [49], where a three-dimensional glide symmetry is imposed in the form of the following constraint:

$$\mathcal{H}(k_x, k_y, k_z) = U\mathcal{H}(-k_x, k_y + \pi, k_z)U^{-1}. \quad (16)$$

This glide symmetry acts analogously to the one above, yielding a Klein bottle topology in the first two coordinates; with the addition of the periodic  $k_z$  direction, the final topology of the Brillouin zone becomes  $K^2 \times S^1$ .

The loss of orientability of the Brillouin zone causes the chiral nature of Weyl nodes to become less well-defined, leading to novel topological features. For example, moving a Weyl

node with Chern number +1 out of the fundamental domain across the  $k_y = -\pi$  plane will cause it to reappear as a Weyl point with Chern number  $-1$  at  $k_y = 0$ . Consequently, the sum of all the Chern numbers associated to the Weyl nodes in the fundamental domain may no longer add to zero, seemingly circumventing the conventional Nielsen–Ninomiya theorem. Instead, Weyl points emerging in a  $K^2 \times S^1$  fundamental domain are found to satisfy an altered  $\mathbb{Z}_2$  cancellation theorem, meaning that over a fundamental domain  $K^2 \times S^1$ , the charges of a set of Weyl points  $W$  are constrained to satisfy

$$\sum_{w_i \in W} \chi_i = 0 \pmod{2}. \quad (17)$$

This has a further natural manifestation in terms of the Fermi arcs on the  $K^2$ -like  $(k_x, k_y)$ -surfaces: instead of only connecting Weyl points of opposite chiralities, Fermi arcs may be bounded by same-chirality Weyl points. Specifically, this is found to occur when a Fermi arc crosses the orientation-reversing  $k_y = 0$  boundary of the surface Brillouin zone an odd number of times; see Fig. 2(c). In the next section, we argue that the physical interpretation of these features is confounded by fixing a specific fundamental domain, and instead develop a coordinate-free formalism based on the (co)homology approach described above.

### 3 Non-orientable (co)homology formalism

The glide symmetry defined in Eq. (16) leads to fascinating topological behaviour, but the discussion of this behaviour is somewhat hampered in the context of a fixed fundamental domain. For example, it is unclear in this context whether the possibly non-zero total charge appearing in the fundamental domain has any implications for the physical properties of the corresponding semimetals. However, as shown in Fig. 3, the total Weyl point charge may depend sensitively on a given parametrisation of the fundamental domain within the Brillouin torus.

To alleviate the potential confusion arising from this choice of fundamental domain, we strive to give an appropriate description of these non-orientable Weyl semimetals in terms of the more coordinate-free (co)homology framework in this section. We will initially treat free orientation-reversing symmetries in full generality, without assuming the specific glide symmetry or the unitarity implicit in Eq. (16).

Before we move on, we include a small note on the Poincaré–Hopf theorem, which is often used to derive the Nielsen–Ninomiya theorem. In the usual setting of a toroidal Brillouin zone  $\mathbb{T}^3$ , the map  $\mathbf{d}(\mathbf{k})$  which sets the Pauli matrix coefficients in the Bloch Hamiltonian [Eq. (1)] can be considered a vector field on  $\mathbb{T}^3$ ; Weyl nodes then correspond to singularities of this vector field. The Poincaré–Hopf theorem then states that the indices of these singularities (i.e. the chiralities of the Weyl nodes) must add to zero. This argument implicitly relies on the fact that the tangent bundle of  $\mathbb{T}^3$  is homeomorphic to the trivial bundle  $\mathbb{T}^3 \times \mathbb{R}^3$  (i.e.  $\mathbb{T}^3$  is *parallelisable*), allowing  $\mathbf{d}(\mathbf{k}) : \mathbb{T}^3 \rightarrow \mathbb{R}^3$  to be identified as a vector field (i.e. a section of the tangent bundle). As such, it does not generalise straightforwardly to other Brillouin zone topologies: for example, the  $K^2 \times S^1$  topology studied in Ref. [49] is not parallelisable, so that  $\mathbf{d}(\mathbf{k}) : K^2 \times S^1 \rightarrow \mathbb{R}^3$  cannot be interpreted as a well-defined vector field. Indeed, the mod 2 charge cancellation found in Ref. [49] is intimately related to the fact that  $\mathbf{d}(\mathbf{k})$  exists on the *orientable* trivial  $\mathbb{R}^3$ -bundle over the *non-orientable* base space  $K^2 \times S^1$  – a point of view which we will not pursue further, in favour of the richer (co)homology interpretation.

The presence of symmetries will generally enforce modifications of the (co)homology treatment introduced in Secs. 2.2 and 2.3. These modifications have been well studied in the more general and more abstract setting of K-theory [43–46, 61], but this is in some sense too blunt

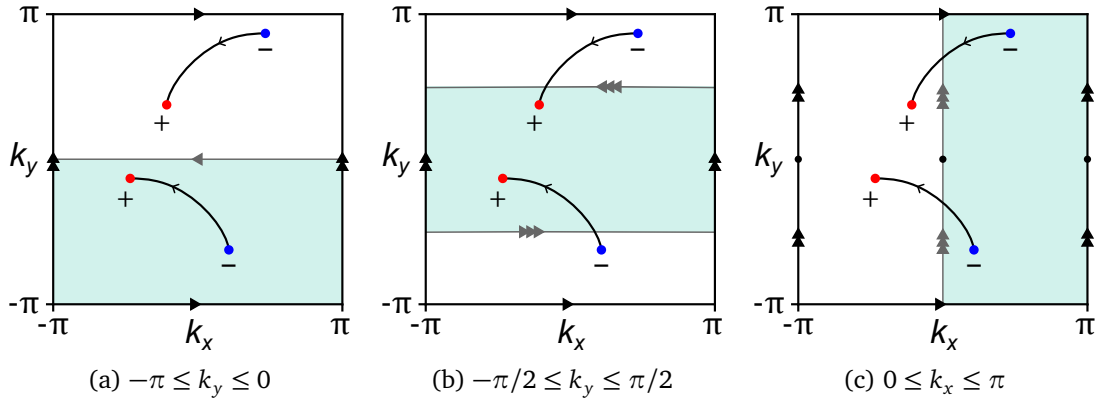


Figure 3: Top view of the three-dimensional Brillouin torus (or two-dimensional surface torus) for a given Weyl semimetal subject to the glide symmetry in Eq. (16). A simple configuration of Weyl nodes is shown, with oriented Dirac strings (Fermi arcs) connecting them. Different parametrisations of the fundamental domain are shaded in teal, all of which take on  $K^2 \times S^1$  ( $K^2$ ) topology after identifying their boundaries along the indicated arrows: (a) the domain outlined in Ref. [49]; (b) the same domain shifted in the  $k_y$  direction; (c) a domain spanning the  $k_y$  direction. Consequently, the notions of both relative and absolute chirality of the two Weyl nodes in the fundamental domain are affected by the choice of parametrisation, indicating that these notions do not have phenomenological implications.

of a tool for our purposes: for Weyl semimetals, a more direct (co)homology interpretation in terms of Weyl points and their concomitant Dirac strings is more computationally tractable, while also offering more direct physical intuition.

The first and most universal of the modifications that additional symmetries impose is the use of *equivariant* (co)homology groups, which encode the action of the relevant symmetry group on the Brillouin torus. For example, the glide symmetry in Eq. (16) has a  $\mathbb{Z}_2$  group action on  $\mathbb{T}^3$ , and the corresponding equivariant second cohomology group  $H_{\mathbb{Z}_2}^2(\mathbb{T}^3)$  classifies glide symmetric Berry curvature 2-forms. These equivariant groups are burdensome to calculate in general, but in special cases where the symmetry group  $G$  has a free action (i.e. one that fixes no specific momenta), they can be reduced to an especially simple form: in this case, they are equivalent to ordinary (co)homology groups on the quotient space  $\mathbb{T}^3/G$  [62]. For the glide symmetry, this quotient space is the aforementioned space  $K^2 \times S^1$ , so that, for example,

$$H_{\mathbb{Z}_2}^2(\mathbb{T}^3) \cong H^2(K^2 \times S^1). \quad (18)$$

In other words, the move to a fully reduced Brillouin zone under a free action is completely justified from a (co)homology perspective. However, the equivalent notion of equivariant (co)homology on the full Brillouin torus is often more physically insightful, and we will often conceptualise groups like  $H^2(K^2 \times S^1)$  as classifying symmetric structures on the full torus.

The other major modification that is required in the case of orientation-reversing symmetries relates to the Poincaré duality that couples the homology and cohomology classifications. The statement of Poincaré duality in Eq. (9) depends explicitly on the orientability of the underlying manifold, and as such is no longer valid in the non-orientable setting. To make full use of both the physical interpretability of cohomology and the natural bulk–boundary correspondence in homology, this duality needs to be restored. This is achieved through the use of so-called *twisted* (co)homology groups, which are calculated in terms of a set of *local coefficients*  $\tilde{\mathbb{Z}}$  that keep track of global changes in orientation across the manifold; this effectively causes orientation-reversing symmetries to act on the (co)homology elements by changing

their sign. These twisted groups give rise to the following two statements of the more general *twisted Poincaré duality* on any  $d$ -dimensional closed manifold, regardless of orientability [57]:

$$H_n(M; \tilde{\mathbb{Z}}) \cong H^{d-n}(M), \quad H^n(M; \tilde{\mathbb{Z}}) \cong H_{d-n}(M), \quad (19)$$

where  $n$  is any integer; that is, either the homology group or the cohomology group, but not both, must be twisted to restore Poincaré duality. In the case where  $M$  is orientable, the local coefficients  $\tilde{\mathbb{Z}}$  are trivial, and both statements reduce to Eq. (9). On a non-orientable manifold, however, twisting either homology or cohomology may lead to fundamentally different groups. As a result, only one of the two twists leads to the correct classification for any given orientation-reversing symmetry, the correct choice depending on the exact nature of the symmetry.

As mentioned in Sec 2.3, the usual Poincaré duality has a natural interpretation in the specific context of Weyl semimetals, in that the orientation of (homological) Dirac strings agrees with the (cohomological) chiralities of the Weyl nodes at their extremities. In this light, we introduce a straightforward heuristic for determining whether the homology or cohomology groups should be twisted; this heuristic is illustrated in detail in Fig. 4. In short, the correct

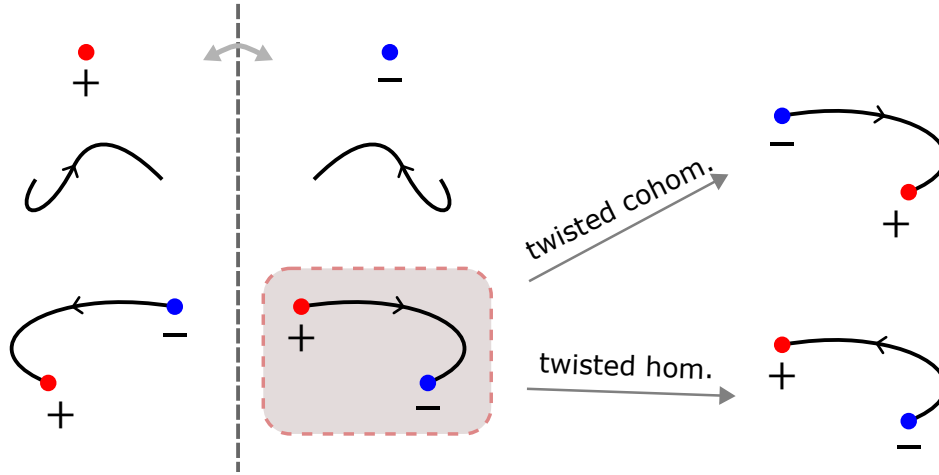


Figure 4: Schematic illustration of the heuristic argument determining which of the (co)homology groups to twist. The top left shows how Weyl point charges [determined by  $H^2(M \setminus W)$ ] and Dirac strings [representing invariants in  $H_1(M, W)$ ] are altered by a change in orientation (represented by the dashed mirror axis). Being a chiral feature, the Weyl point charge is reversed; meanwhile, the internal orientation of the Dirac string is maintained, despite the string itself being mirrored (i.e. its image is also oriented away from the “hook” at the end). As a result, use of ordinary (co)homology groups leads to constructions (shown in the shaded area) where the orientation Dirac string may disagree with the chiralities of the two Weyl nodes it connects – this is a result of Poincaré duality breaking. The duality is restored by twisting either the cohomology or the homology, effectively undoing the chirality reversal or reversing the orientation of the Dirac string, respectively. The correct choice between the two then depends on the way in which the orientation-reversing symmetry is observed to act on Weyl nodes in the system: symmetric pairs of opposite (same) chirality indicate twisted (co)homology.

choice of twist may be inferred by studying the relative charges of pairs of Weyl nodes that are related by the orientation-reversing symmetry. Since these charges are both cohomological and chiral in nature, the symmetry is expected to reverse their sign under ordinary cohomology; that is, if a symmetric pair of Weyl nodes has opposite charges, this indicates that ordinary

cohomology (and, by extension, twisted homology) must be used to describe the system. Conversely, if both Weyl nodes in the pair have the same chirality, then the correct description is given using twisted cohomology and ordinary homology.

All orientation-reversing symmetries considered in the rest of this work [notably including the glide symmetry in Eq. (16)] will be unitary, which directly constrains the symmetric partners of Weyl nodes to be of the opposite chirality. This can be seen from the integral in Eq. (3): the Berry curvature in the integrand is itself invariant under unitary transformations of the Hamiltonian [63], whereas a reversed orientation of the integration domain  $S^2$  leads to a single sign change. It follows that all unitary orientation-reversing symmetries lead to classification by ordinary cohomology and twisted homology. We will refer to the Dirac strings and loops in these twisted homology groups as *twisted Dirac strings* and *twisted Dirac loops*, to emphasise that they do not admit a consistent orientation within a non-orientable Brillouin zone; an example of this can be seen in the different fundamental domains in Fig. 3.

In contrast to this, anti-unitary orientation-reversing symmetries may in some cases give rise to same-charge symmetric pairs of Weyl nodes. Most notably, this is the case under time reversal symmetry, which induces an orientation-reversing inversion on the Brillouin zone; as the heuristic argument in Fig. 4 would suggest, time-reversal symmetric semimetals are indeed properly classified using twisted cohomology and untwisted homology [47].

As a final note, we must stress that the formalism laid out above only provides a complete classification in the case when the orientation-reversing symmetry has a free action; if instead the action has fixed momenta, then additional arguments must be given to determine the role that those momenta play in the (co)homology classification. We will explore a heuristic approach to such arguments in the important case of inversion-symmetric Weyl semimetals in Sec. 5.3.

## 4 Topology of $K^2 \times S^1$

We now have the necessary tools to formulate the coordinate-free topological description of Weyl semimetals subject to the glide symmetry given by Eq. (16). Following the reasoning of Sec. 3, Poincaré duality is restored by imposing a twist in the homology groups. Hence, the following sequence in ordinary cohomology groups is employed, where we notate  $M := K^2 \times S^1$ :

$$0 \rightarrow \underbrace{H^2(M)}_{\text{Insulator}} \rightarrow \underbrace{H^2(M \setminus W)}_{\text{Semimetal}} \rightarrow \underbrace{\bigoplus_{w \in W} H^2(S_w^2)}_{\text{Local charges}} \xrightarrow{\Sigma} \underbrace{H^3(M)}_{\text{Total charge}} \rightarrow 0. \quad (20)$$

Equivalently, the Poincaré dual sequence in twisted homology groups reads

$$0 \rightarrow \underbrace{H_1(M; \tilde{\mathbb{Z}})}_{\text{Twisted Dirac loops}} \rightarrow \underbrace{H_1(M, W; \tilde{\mathbb{Z}})}_{\text{Twisted Dirac strings}} \xrightarrow{\partial} H_0(W; \tilde{\mathbb{Z}}) \xrightarrow{\Sigma} H_0(M; \tilde{\mathbb{Z}}) \rightarrow 0. \quad (21)$$

Since Eq. (20) is given in terms of ordinary cohomology groups, it can be readily calculated using standard tools in algebraic topology, for instance employing cellular homology [57]. The sequences explicitly read

$$0 \rightarrow \mathbb{Z} \oplus \mathbb{Z}_2 \xrightarrow{\alpha} \mathbb{Z} \oplus \mathbb{Z}_2 \oplus \mathbb{Z}^k \xrightarrow{\beta} \mathbb{Z}^k \xrightarrow{\Sigma} \mathbb{Z}_2 \rightarrow 0, \quad (22)$$

with  $k$  being the total number of Weyl points. In what follows, we discuss the topological and physical consequences of this sequence.



#### 4.1 Mod 2 charge cancellation

Before explicitly discussing the topological invariants and their nature, we will address the coordinate-free version of the main result of Ref. [49], namely the mod 2 charge cancellation condition. This condition relates directly to the fact that the rightmost group in the sequence Eq. (22) is  $\mathbb{Z}_2$ . This is a completely general feature for non-orientable manifolds; the group appearing here is the top cohomology group, and  $H^n(M) = \mathbb{Z}_2$  for any  $n$ -dimensional non-orientable manifold  $M$ .

Recall that in the orientable case, charge cancellation is obtained from the sequence in Eq. (8) by noting that exactness forces the Weyl point charges in  $\mathbb{Z}^k$  to sum to  $0 \in \mathbb{Z}$  whenever they descend from a semimetal phase. The reasoning is similar in the non-orientable case, but one needs to be a bit more careful in the sense that the group  $\mathbb{Z}^k$  appearing in Eq. (22) no longer admits a canonical basis. Concretely, the group  $H^2\left(\bigcup_{i=1}^k S_{w_i}^2\right) \cong \mathbb{Z}^k$  and its dual  $H_0(W; \tilde{\mathbb{Z}})$  cannot be directly interpreted as Weyl point charges, since the spheres surrounding the Weyl points no longer have a canonically defined orientation induced by the manifold  $M$ . Indeed, fixing a basis for this group is equivalent to fixing a specific orientation at each Weyl point, a choice that is directly related to the freedom to choose different fundamental domains in the manner illustrated in Fig. 3. Importantly, however, the map  $\Sigma$  acts as a well-defined sum of the entries in this  $\mathbb{Z}^k$ , independently of this choice of basis: precisely because it maps onto  $\mathbb{Z}_2$ , it is invariant under changes of orientation ( $\chi \equiv -\chi \pmod{2}$ ). Therefore, we can write

$$\Sigma : \mathbb{Z}^k \rightarrow \mathbb{Z}_2, \quad (\chi_1, \dots, \chi_k) \mapsto \sum_{i=1}^k \chi_i \pmod{2} \quad (23)$$

without fixing the sign of each  $\chi_i$  in advance.

With this knowledge in hand, the argument proceeds similarly to the orientable case: since the sequence is exact, charges initially belonging to a semimetal structure [which are therefore mapped into  $\mathbb{Z}^k$  by the map  $\beta$  in Eq. (22)] necessarily add to  $0 \in \mathbb{Z}_2$  in any basis. This is the precise coordinate-free interpretation of the mod 2 charge cancellation theorem presented in Eq. (23), stemming from Ref. [49]. Importantly, note that our construction imposes meaningful limits on the interpretation of this charge cancellation: on the one hand, the lack of a canonical basis represents an unphysical degree of freedom, implying that there is no physical interpretation in terms of a particular non-zero total charge; on the other hand, the appearance of  $H^3(K^2 \times S^1) \cong \mathbb{Z}_2$  ensures that such an interpretation is also not mathematically meaningful, since the total charge is fundamentally a  $\mathbb{Z}_2$  invariant.

Beyond this charge cancellation theorem, the exactness of the sequence Eq. (22) also allows us to conclude the converse: if any charge configuration in  $\mathbb{Z}^k$  adds to  $0 \in \mathbb{Z}_2$ , it necessarily admits a semimetal configuration. Concretely, this means that any combination of charges inside a given fundamental domain that has an even total can be realised in a Weyl semimetal phase.

#### 4.2 Topological invariants

As mentioned in Secs. 2.2 and 2.3, Weyl semimetals can be considered transitional phases between different insulating phases, and their topology can be understood in terms of insulating invariants. As such, understanding the set of semimetal invariants on  $K^2 \times S^1$  begins with a good grasp of the insulating invariants. These invariants are classified by the first group appearing in Eqs. (20), (21) and (22), namely the group

$$H^2(K^2 \times S^1) \cong H_1(K^2 \times S^1; \tilde{\mathbb{Z}}) \cong \mathbb{Z} \oplus \mathbb{Z}_2 \quad (24)$$

In contrast to the conventional three-dimensional insulating topology, which is given by three Chern numbers  $C_i \in \mathbb{Z}$  stemming from  $H^2(\mathbb{T}^3) \cong \mathbb{Z}^3$ , the insulating phases on  $K^2 \times S^1$  are

classified by just two invariants: one  $\mathbb{Z}$  invariant  $\nu_x$  and one  $\mathbb{Z}_2$  invariant  $\nu_z$ . These invariants can be most intuitively understood by studying how the glide symmetry acts on the Dirac loops in  $H_1(\mathbb{T}^3)$  to give twisted Dirac loops in  $H_1(K^2 \times S^1; \tilde{\mathbb{Z}})$ .

Dirac loops are formed when Weyl points are annihilated along topologically non-trivial paths in the Brillouin zone. In the absence of any symmetries, the insulating homology group  $H_1(\mathbb{T}^3) \cong \mathbb{Z}^3$  is generated by the homology classes of the three basic Dirac loops spanning the different coordinate directions of the Brillouin torus; we denote these loops by  $\ell_i$  with  $i \in \{x, y, z\}$ . As explained in Sec. 2.3, these loops are precisely dual to the three insulating Chern numbers  $\mathbf{C} = (C_x, C_y, C_z)$  defined in Eq. (7). The glide symmetry induces a symmetric partner  $\ell'_i$  to each of these loops, and their respective sums  $\tilde{\ell}_i = \ell_i + \ell'_i$  represent elements in the twisted homology group  $H_1(K^2 \times S^1; \tilde{\mathbb{Z}})$ , due to the equivalence between homology on  $K^2 \times S^1$  and equivariant homology on  $\mathbb{T}^3$  mentioned in Sec. 3; this construction is illustrated in Fig. 5. Together, these three twisted Dirac loops generate the two invariants mentioned

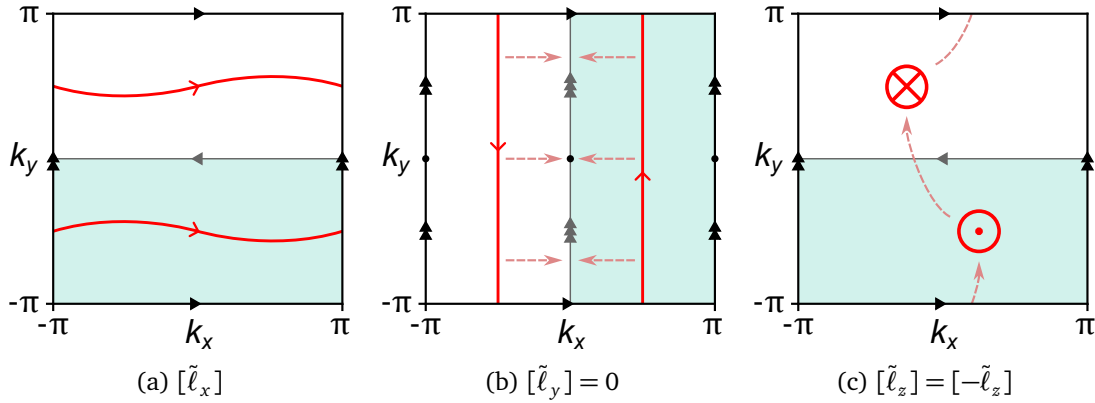


Figure 5: Top view of the  $\mathbb{T}^3$  Brillouin torus. Each of the three basic Dirac loops  $\ell_i$  are shown contained within an appropriately chosen  $K^2 \times S^1$  fundamental domain (shaded teal), and doubled by glide symmetry to the other half of the torus. The combined structure (shown in red) can be regarded as a twisted Dirac loop  $\tilde{\ell}_i$  [representing an invariant in  $H_1(K^2 \times S^1; \tilde{\mathbb{Z}})$ ] in each instance. (a) For  $\ell_x$ , the parity change induced by  $k_x \mapsto -k_x$  is cancelled out by the orientation reversal induced by the twist in the homology. The resulting twisted Dirac string  $\tilde{\ell}_x$  thus has a consistent orientation, and the associated invariant  $\nu_x \in \mathbb{Z}$  induces an even Chern number  $C_x = 2\nu_x \in 2\mathbb{Z}$  on the full torus. (b) For the case of  $\ell_y$ , the corresponding twisted Dirac loop  $\tilde{\ell}_y$  is trivial: the mirroring along  $k_x = 0$  and subsequent orientation reversal result in a set of two oppositely orientated loops. These loops can be brought together along the dashed arrows in a symmetry-preserving fashion, eventually cancelling when they meet on the glide plane. As a result, there is no invariant  $\nu_y$ . (c) The Dirac loop  $\ell_z$  running in the positive  $k_z$  direction (“out of the page”) in the fundamental domain is doubled to a second loop running in the negative  $k_z$  direction (“into the page”). These loops cannot be merged in a fashion consistent with the symmetry, but they can instead be permuted along the dashed arrows. As a consequence, the resulting twisted Dirac string  $\tilde{\ell}_z$  is equivalent to its own inverse  $-\tilde{\ell}_z$ ; that is,  $\tilde{\ell}_z$  generates a  $\mathbb{Z}_2$  invariant  $\nu_z$ .

above:  $\tilde{\ell}_x$  generates the  $\mathbb{Z}$  invariant  $\nu_x$ ,  $\tilde{\ell}_y$  is topologically trivial, and  $\tilde{\ell}_z$  generates the  $\mathbb{Z}_2$  invariant  $\nu_z$ . Of these, the  $\mathbb{Z}_2$  invariant  $\nu_z$  is closely related to the  $\mathbb{Z}_2$  invariant found on the two-dimensional Klein bottle  $K^2$  in Ref. [50], and its appearance and properties in the semimetallic  $K^2 \times S^1$  context has been discussed in detail in Ref. [49].

The  $\mathbb{Z}$  invariant  $\nu_x$  has not been previously reported; in the insulating context it can be

naively calculated as half of the Chern number  $C_x$  appearing in Eq. (7):

$$\nu_x = \frac{1}{2}C_x = \frac{1}{4\pi} \int_{\mathbb{T}_{k_x=\text{const.}}^2} \mathcal{F}. \quad (25)$$

This integral, despite not necessarily respecting the glide symmetry, yields a consistent value because the symmetry precisely doubles  $\ell_x$ -like Dirac loops.

In the presence of Weyl nodes, the group of invariants is instead given by the semimetal group

$$H^2(K^2 \times S^1 \setminus W) \cong H_1(K^2 \times S^1, W; \tilde{\mathbb{Z}}) \cong \mathbb{Z} \oplus \mathbb{Z}_2 \oplus \mathbb{Z}^k, \quad (26)$$

where  $k = |W|$  is the number of Weyl points. The structure of this group is reminiscent of the  $\mathbb{Z}^3 \oplus \mathbb{Z}^{k-1}$  group appearing in the orientable case in Eq. (8), in that it combines the insulating topology with a set of Weyl point charge configurations. The one crucial difference is that these charge configurations are represented by a  $\mathbb{Z}^k$  subgroup rather than  $\mathbb{Z}^{k-1}$ , reflecting the weaker mod 2 charge cancellation condition. Physically, this implies that a single Weyl point on  $K^2 \times S^1$  may give rise to valid semimetal topology, as opposed to the minimum of two Weyl points that are necessary in the orientable case. Such a lone Weyl point necessarily has an even charge, enforced by the mod 2 charge cancellation; this was also pointed out in the supplement to Ref. [49].

Just as in conventional Weyl semimetals, the Weyl points serve as singularities of the Berry flux; as a result, the invariant on a two-dimensional slice of the Brillouin zone is modified by an amount dictated by the Weyl point charge. This modification has to be treated with care in the non-orientable case, in a way which respects the glide symmetry on the Brillouin zone. This is true in particular in the case of  $\nu_x$ ; as mentioned above, the integral in Eq. (25) does not necessarily respect the glide symmetry. This does not lead to any issues in the insulating case, but as illustrated in Fig. 6(a), it may lead to unphysical results in the semimetallic case. Along the same line as for time-reversal symmetric systems, where integrals have to be taken over  $\mathcal{T}$ -invariant surfaces [47], the integral instead needs to be taken over a surface  $S$  that preserves the glide symmetry and is continuously deformable into a surface of constant  $k_x$ ; see Fig. 6(b). In principle, only the half of the surface  $S$  that intersects the fundamental domain at  $k_y \leq 0$

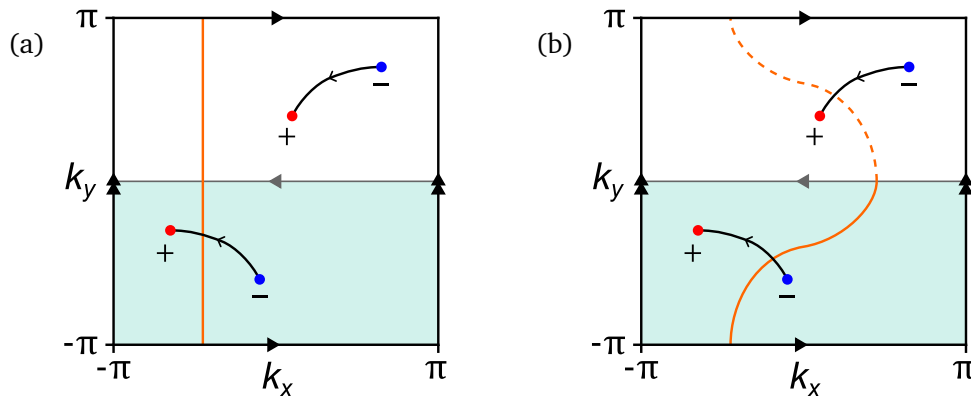


Figure 6: Incorrect (a) and correct (b) calculations of the  $\nu_x$  invariant in a given setting. (a) In a given semimetal, the slice of constant  $k_x$  (orange) appearing in Eq. (25) may only intersect a single Dirac string, yielding the non-integer value of  $1/2$  in the pictured setup. (b) If integration is instead carried out over a topologically equivalent glide symmetric surface, the topological invariant  $\nu_x$  is well-defined outside of Weyl points. The dashed half of the surface is redundant, since it yields the same integral as the solid half. The pictured setup yields  $\nu_x = 1$ .

needs to be integrated over; this half can be considered a compact subspace of  $K^2 \times S^1$ . The explicit calculation can thus be written as

$$\nu_x = \frac{1}{2\pi} \int_{S_{1/2}} \mathcal{F}, \quad (27)$$

where  $S_{1/2}$  denotes the appropriate half of the surface  $S$ . This integration domain may be continuously deformed while respecting the symmetry. As alluded to above, passing it over a Weyl point with charge  $\chi$  alters  $\nu_x$  to a new value of  $\nu'_x = \nu_x \pm \chi$ , with the choice of sign depending on the direction in which the Weyl point passes through the surface.

The  $\mathbb{Z}_2$  invariant  $\nu_z$  is somewhat more lenient with respect to the choice of surface: since the glide symmetric partner of a Weyl node always has the same  $k_z$ -value, this invariant may consistently be calculated on slices of constant  $k_z$ , as is done in Ref. [49]. This invariant obeys a similar rule to  $\nu_x$  with respect to different integration domains: letting a constant- $k_z$  slice with associated  $\mathbb{Z}_2$ -invariant  $\nu_z$  pass over a Weyl point with charge  $\chi$  along the  $k_z$ -direction, the new  $\mathbb{Z}_2$ -invariant becomes  $\nu'_z = \nu_z + \chi \pmod{2}$ . It should be emphasised that no  $\mathbb{Z}_2$  charge needs to be assigned to each individual Weyl point to support this behaviour, contrary to the description in Ref. [49]. This is reflected in the structure of the semimetal group in Eq. (26): the only  $\mathbb{Z}_2$  factor in this group stems from the underlying insulating topology, and the addition of any Weyl points only contributes additional  $\mathbb{Z}$  factors. That is, no  $\mathbb{Z}_2$  topology is intrinsically associated with the Weyl point charge. A comparable construction appears in the case of time-reversal symmetric Weyl semimetals: there, Weyl points also mediate a  $\mathbb{Z}_2$  invariant without having intrinsic  $\mathbb{Z}_2$  topology [47].

### 4.3 $K^2$ surface states

Having focused exclusively on the description of the bulk topology above, we now turn our attention to the classification of the corresponding boundary states on the non-orientable  $(k_x, k_y)$ -surface. These states are obtained by performing a projection  $\pi_z$  along the periodic  $k_z$  direction, effectively integrating out the  $S^1$  factor in  $K^2 \times S^1$ ; the resulting surface Brillouin zone then has the topology of  $K^2$ . Just as in the bulk, the lack of a consistent choice of orientation leads the chirality of the surface states (i.e. the Fermi arcs) to be ill-defined; as such, a coordinate-free description offers similar insights in this setting.

The description of surface topology is obtained by letting the projection  $\pi_z$  act on homology classes, analogous to the construction in Sec. 2.4. Concretely, any given twisted relative homology class  $[c] \in H_1(K^2 \times S^1, W; \tilde{\mathbb{Z}})$  is represented by a configuration of twisted Dirac strings  $c$ . The surface projection  $\pi_z$  naturally preserves the twisted orientation of such configurations, allowing a well-defined pushforward  $(\pi_z)_*$  on twisted homology classes:

$$(\pi_z)_* : H_1(K^2 \times S^1, W; \tilde{\mathbb{Z}}) \rightarrow H_1(K^2, W'; \tilde{\mathbb{Z}}), \quad [c] \mapsto [\pi_z(c)], \quad (28)$$

where  $W'$  denotes the projected surface Weyl nodes as before. Similarly to the orientable case, these surface homology classes are exactly represented by the physical Fermi arcs. Given the correct orientation, it is therefore appropriate to think of these structures in terms of *twisted Fermi arcs*. Furthermore, the pushforward  $(\pi_z)_*$  is a surjective map, ensuring that all physically realisable Fermi arc configurations on  $K^2$  are classified by the group  $H_1(K^2, W'; \tilde{\mathbb{Z}})$ .

Just as in the orientable case, the pushforward construction may be extended to the entire homology sequence in Eq. (21), yielding the following exact sequence on the surface:

$$0 \rightarrow \underbrace{H_1(K^2; \tilde{\mathbb{Z}})}_{\text{Twisted Fermi loops}} \rightarrow \underbrace{H_1(K^2, W'; \tilde{\mathbb{Z}})}_{\text{Twisted Fermi arcs}} \xrightarrow{\partial} H_0(W'; \tilde{\mathbb{Z}}) \rightarrow H_0(K^2; \tilde{\mathbb{Z}}) \rightarrow 0. \quad (29)$$

For calculational purposes, it is beneficial to employ twisted Poincaré duality on the surface in order to recover a Mayer–Vietoris sequence in terms of more tractable untwisted cohomology groups:

$$\cdots \xrightarrow{0} H^1(K^2) \rightarrow H^1(K^2 \setminus W') \rightarrow \bigoplus_{w' \in W'} H^1(S_{w'}^1) \rightarrow H^2(K^2) \rightarrow 0. \quad (30)$$

Again, the use of first rather than second cohomology signifies that the surface invariants are calculated in terms of winding numbers of a Berry connection 1-form, rather than Chern numbers.

Just as in the bulk, the groups in Eq. (30) can be straightforwardly calculated using e.g. cellular homology, resulting in the following explicit sequence:

$$\cdots \xrightarrow{0} \mathbb{Z} \rightarrow \mathbb{Z} \oplus \mathbb{Z}^k \rightarrow \mathbb{Z}^k \xrightarrow{\Sigma} \mathbb{Z}_2 \rightarrow 0. \quad (31)$$

This sequence is more or less identical in form and interpretation to the bulk sequence in Eq. (22); the only essential difference is that the  $\mathbb{Z}_2$ -factor corresponding to the invariant  $\nu_z$  is missing as a consequence of projecting along the  $k_z$ -direction. As a result, the  $K^2$  surface is subject to analogous mod 2 charge cancellation, admitting the same interpretation as in Sec. 4.1. In particular, the lack of a canonical basis for  $H^1(K^2 \setminus W') \cong \mathbb{Z}^k$  implies that the chirality of individual surface Weyl nodes is fundamentally ill-defined, as is the relative chirality between them. Physically, this means that different parametrisations of the fundamental domain can be used to obtain seemingly different Fermi arc structures.

This ambiguity with respect to different parametrisations helps explain the experimental results in Ref. [49], where two surface Weyl nodes are found to have the same chirality with respect to a given  $K^2$  fundamental domain. Explicitly, this is probed by measuring the dispersion along two loops encircling the surface projections of two positive Weyl nodes. In light of the results obtained here, this observation is highly dependent on the choice of fundamental domain and can be altered through a reparametrisation; this is illustrated in more detail in Fig. 7.

Finally, the sequence in Eq. (31) has a natural interpretation in terms of two-dimensional non-Hermitian systems; this correspondence is explored in greater depth in Sec. 5.2.

## 5 Extensions

The formalism for topological classification under orientation-reversing symmetries introduced in Sec. 3 is formulated in very general terms, and has many potential applications beyond the  $K^2 \times S^1$  system studied in Sec. 4. Three such applications are studied in this section: we classify the complete set of possible non-orientable Brillouin zones and their associated invariants (Sec. 5.1), discuss extensions to the topology of exceptional points in non-Hermitian systems (Sec. 5.2), and use a heuristic ansatz to arrive at a classification scheme for the experimentally important class of Weyl semimetals subject to inversion symmetry (Sec. 5.3).

### 5.1 Additional non-orientable Brillouin zones

The three-dimensional glide symmetry studied in Sec. 4 is not the only space group symmetry with free action resulting in a non-orientable fundamental domain. To identify what further symmetries are of relevance in this aspect, we recall that there are a total of 230 space groups in three dimensions. Most of these symmetries induce fixed momenta on the torus: only 13 (including the trivial group) have a free action, allowing them to induce proper reduced Brillouin zones [64]. A further four of these symmetries are orientation-reversing, in that they

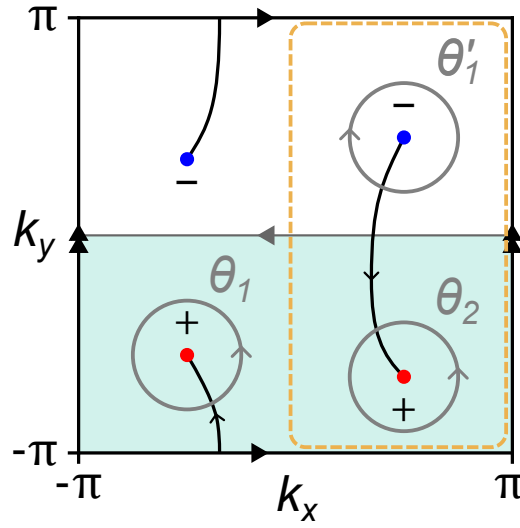


Figure 7: Schematic contextualisation of the experiment carried out in Ref. [49], where the surface dispersion is measured along the loops  $\theta_1$  and  $\theta_2$  encircling the projections of two positive Weyl nodes onto a  $K^2$  fundamental domain (shaded teal). This measurement yields two surface states of the same apparent chirality. Upon reparametrisation to the alternative fundamental domain outlined in orange, the loop  $\theta_1$  is mirrored to a different loop  $\theta'_1$  by the glide symmetry, which encircles the projection of a negative Weyl node in the clockwise direction. This change in orientation counteracts the change of chirality of the corresponding Weyl node, so that the dispersion along  $\theta'_1$  is identical to that along  $\theta_1$ . Returning  $\theta'_1$  to the conventional counterclockwise orientation yields the expected dispersion of a surface state with negative chirality; as a result, the alternative fundamental domain will be found to feature two oppositely charged points connected by a Fermi arc displaying conventional dispersion characteristics.

include at least one glide symmetry; the other eight non-trivial free-acting groups are all generated by orientation-preserving screw rotations (i.e. combinations of rotation and fractional lattice translation). These four groups are precisely the ones which give rise to a non-orientable Brillouin zone.

The simplest of these four groups is  $Pc$ , which is generated by a single glide symmetry; this is exactly the case treated in detail in Sec. 4 above. The remaining three groups are  $Cc$ ,  $Pca2_1$ , and  $Pna2_1$ , and all of them combine a glide symmetry with another  $\mathbb{Z}_2$  operation. As a consequence, these three groups are homomorphic to  $\mathbb{Z}_2 \oplus \mathbb{Z}_2$ , as opposed to the  $\mathbb{Z}_2$  corresponding to  $Pc$ . It follows that their respective fundamental domains cover a quarter of the Brillouin torus rather than half of it; see Fig. 8. Just as in the case of  $K^2 \times S^1$ , all of these fundamental domains attain the topology of a three-dimensional non-orientable manifold when their boundaries are identified according to the action of the symmetry. These spaces are more complex in nature than  $K^2 \times S^1$ , and as such they do not necessarily have standard names; they are best conceptualised in terms of the action of the symmetry itself. Notably, the boundary identifications which give rise to these spaces naturally induce cell structures on the fundamental domain; these cell structures can be used to calculate the relevant exact sequences of invariants using cellular homology. Below, we will assume that all these symmetries are made to act unitarily on the momentum-space Brillouin torus;  $U_X$  will denote unitary representations of all symmetry generators. As mentioned in Sec. 3, this ensures that the correct topological description is given in terms of ordinary cohomology and twisted homology. For each symmetry, we list the precise action on the momentum-space Hamiltonian, together with the explicitly calculated



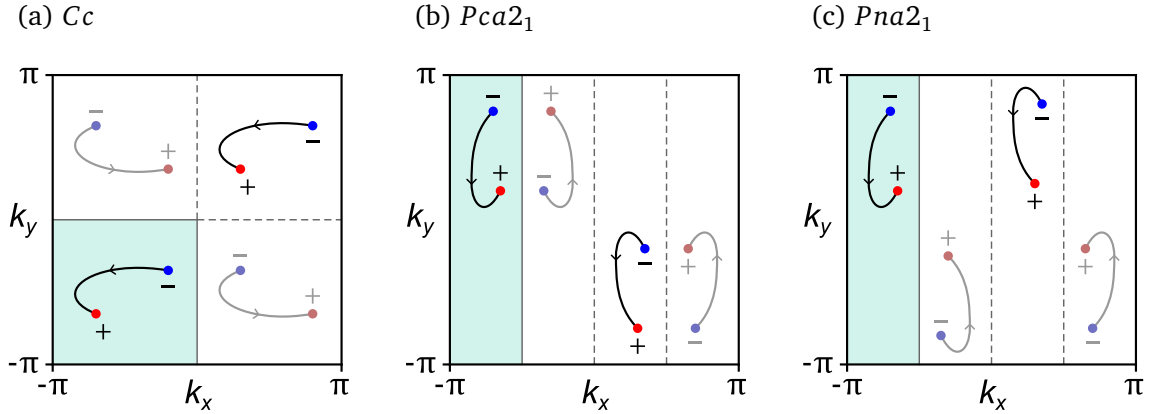


Figure 8: Top view of the Brillouin torus  $\mathbb{T}^3$ , subject to the space group symmetries (a)  $Cc$ , (b)  $Pca2_1$ , and (c)  $Pna2_1$ . In each case, an arbitrary choice of fundamental domain is given (shaded teal). To help illustrate the action of each symmetry, a structure consisting of a Dirac string connecting two Weyl nodes is placed in this fundamental domain; three symmetric copies of this structure then appear in other sections of the Brillouin torus. Greyed-out structures indicate copies that have been translated by  $\pi$  in the  $k_z$ -direction with respect to the original, and thus do not lie on the same  $k_z$ -plane. The fundamental domains shown are made into non-orientable spaces by identifying the elements of their boundary which are related by the symmetry. These identifications give rise to cell structures, which can be used to calculate groups of invariants via cellular homology. Importantly, these groups are independent of the choice of fundamental domain.

semimetal Mayer–Vietoris sequence belonging to the system.

First, the  $Cc$  group combines a glide symmetry and a diagonal half-lattice translation, resulting in symmetry constraints on the Hamiltonian reading

$$\mathcal{H}(k_x, k_y, k_z) = U_{Cc_1} \mathcal{H}(k_x, -k_y, k_z + \pi) U_{Cc_1}^{-1}, \quad (32)$$

$$\mathcal{H}(k_x, k_y, k_z) = U_{Cc_2} \mathcal{H}(k_x + \pi, k_y + \pi, k_z) U_{Cc_2}^{-1}. \quad (33)$$

The Mayer–Vietoris sequence in ordinary cohomology (equivalently, the exact sequence in twisted homology) is as follows:

$$0 \rightarrow \mathbb{Z} \oplus \mathbb{Z}_2^2 \rightarrow \mathbb{Z} \oplus \mathbb{Z}_2^2 \oplus \mathbb{Z}^k \rightarrow \mathbb{Z}^k \rightarrow \mathbb{Z}_2 \rightarrow 0. \quad (34)$$

Second, the group  $Pca2_1$  is generated by a combined glide reflection and screw rotation, which manifest in momentum space as

$$\mathcal{H}(k_x, k_y, k_z) = U_{(Pca2_1)_1} \mathcal{H}(k_x + \pi, -k_y, k_z) U_{(Pca2_1)_1}^{-1}, \quad (35)$$

$$\mathcal{H}(k_x, k_y, k_z) = U_{(Pca2_1)_2} \mathcal{H}(-k_x, -k_y, k_z + \pi) U_{(Pca2_1)_2}^{-1}, \quad (36)$$

and give rise to the following sequence:

$$0 \rightarrow \mathbb{Z}_2^2 \rightarrow \mathbb{Z}_2^2 \oplus \mathbb{Z}^k \rightarrow \mathbb{Z}^k \rightarrow \mathbb{Z}_2 \rightarrow 0. \quad (37)$$

Finally, the  $Pna2_1$  group is formed by operations similar to those defining  $Pca2_1$ , but with an offset in the glide reflection plane from  $k_y = 0$  to  $k_y = \pm\pi/2$ . The corresponding symmetry relations are

$$\mathcal{H}(k_x, k_y, k_z) = U_{(Pna2_1)_1} \mathcal{H}(k_x + \pi, \pi - k_y, k_z) U_{(Pna2_1)_1}^{-1}, \quad (38)$$

$$\mathcal{H}(k_x, k_y, k_z) = U_{(Pna2_1)_2} \mathcal{H}(-k_x, -k_y, k_z + \pi) U_{(Pna2_1)_2}^{-1}, \quad (39)$$

with a Mayer–Vietoris sequence of the form

$$0 \rightarrow \mathbb{Z}_4 \rightarrow \mathbb{Z}_4 \oplus \mathbb{Z}^k \rightarrow \mathbb{Z}^k \rightarrow \mathbb{Z}_2 \rightarrow 0. \quad (40)$$

The non-orientable Brillouin zones induced by all of the above space group symmetries naturally obey the same mod 2 charge cancellation theorem as seen on  $K^2 \times S^1$ , as can be seen from similar features of the exact sequences: the final group of total charge is  $\mathbb{Z}_2$  in each case, and the second group of semimetal invariants has a factor of  $\mathbb{Z}^k$  rather than  $\mathbb{Z}^{k-1}$  relating to Weyl point charges.

The difference between the various space groups instead manifests itself via the group of insulating invariants, reflecting the fact that the reduced Brillouin zones have fundamentally different topologies under each symmetry. As the main focus in this work is on qualitative semimetallic topology, providing explicit expressions for these insulating topological invariants is beyond the current scope. It should be stressed, though, that physical intuition on these invariants can be drawn from arguments related to twisted homology groups and twisted Dirac strings, similarly to the procedure illustrated in Fig. 5.

Finally, a more technical treatment of these symmetries in terms of spectral sequences in K-theory is provided in Ref. [46], in the context of the complete set of 230 space groups.

## 5.2 Non-Hermitian systems

As recent years have seen a vastly increased focus on the topology of operators in the non-Hermitian regime, paving the way to the field of non-Hermitian topological physics [65], we would be remiss not to include a discussion of the way in which our coordinate-free topological classification extends to these systems. In non-Hermitian systems, the conventional Weyl points are replaced by so-called exceptional points, marking degeneracies at which not only the eigenvalues (i.e. the energy bands), but also the eigenvectors (i.e. the eigenstates of the Hamiltonian) coalesce [66]. Remarkably, the generic appearance of these exceptional points requires the tuning of only two parameters; as a result, they may already appear as stable points in two dimensions, in contrast to Weyl points which require three dimensions to appear generically. Non-Hermitian systems subject to orientation-reversing symmetries were recently studied in Refs. [54, 55], where the authors show that some of the conclusions valid in Hermitian systems carry over into the non-Hermitian regime. However, the problems arising from the lack of orientability remain, once again motivating the need for an extended and coordinate-free topological classification of these systems.

Fortunately, certain important classes of non-Hermitian systems can be mapped canonically onto corresponding Hermitian semimetals, allowing the topology to be studied directly using the tools developed above. The key concepts at work in this correspondence are the so-called *resultant winding number* [67–69] and *resultant Hamiltonian* [70], which can be employed to relate the topology of non-Hermitian exceptional points to that of Hermitian nodal points. The most important concepts will be repeated here, but the reader is referred to Refs. [69, 70] for a more detailed background on this matter. In the rest of this section, we employ a two-dimensional glide symmetry as an illustrative example.

A non-Hermitian Hamiltonian subject to a two-dimensional glide symmetry is bound to satisfy

$$\mathcal{H}(k_x, k_y) = U \mathcal{H}(-k_x, k_y + \pi) U^{-1}. \quad (41)$$

This Hamiltonian may generically host exceptional points, the location of which can be derived from its characteristic polynomial: in general, specific resultants of this polynomial and its derivatives will be zero at such points. The characteristic polynomial is given by  $P_2(\lambda; \mathbf{k}) = \det[\mathcal{H}(\mathbf{k}) - \lambda I]$ , and the corresponding resultant is given by

$$R(\mathbf{k}) = \text{Res}[P_2(\lambda; \mathbf{k}), \partial_\lambda P_2(\lambda; \mathbf{k})]. \quad (42)$$

This resultant is complex-valued in general, meaning it gives rise to a well-defined vector field on the two-dimensional Brillouin zone:

$$\mathbf{R}(\mathbf{k}) = \{\text{Re}[R(\mathbf{k})], \text{Im}[R(\mathbf{k})]\}. \quad (43)$$

The zeros of  $\mathbf{R}$  then correspond exactly to the position of the exceptional points [69, 70]. Importantly,  $\mathbf{R}(\mathbf{k})$  satisfies the same two-dimensional glide symmetry as the parent Hamiltonian, meaning that the topology of the zeros of  $\mathbf{R}(\mathbf{k})$  (and hence the topology of the exceptional points of the parent Hamiltonian) can be described using a Mayer–Vietoris sequence coinciding with Eq. (30). Therefore, the same mod 2 charge cancellation theorem readily holds for exceptional points in non-Hermitian systems in two dimensions, as well as the corresponding conclusions regarding reparametrisations of the fundamental domain. The conclusions regarding the  $K^2$  surface Fermi arcs stemming from Sec. 4.3 are instead carried over to a completely analogous interpretation of the uniquely non-Hermitian bulk Fermi arcs, which are branch-cut like curves connecting exceptional points.

One fundamental limitation of this formalism should be pointed out: due to the commutative nature of (co)homology groups, it only captures Abelian topology in non-Hermitian systems, whereas such systems may host non-Abelian topology in general. To be specific, this Abelian topology arises in the context of  $n$ -fold exceptional points emerging in  $n$ -band systems; for example, the Hamiltonian discussed above therefore needs to describe a two-band system, as exceptional points generically emerging in two dimensions are two-fold degenerate [65].

### 5.3 Inversion symmetry

As a last extension, we will outline a heuristic approach to the (co)homological classification of inversion-symmetric Weyl semimetals. This type of Weyl semimetal is of marked experimental importance, since a material needs to break either time reversal or inversion symmetry in order to host Weyl nodes [6], but not necessarily both. Given that time reversal symmetry is naturally broken in the presence of a magnetic field, some prominent experimental realisations of Weyl semimetals have come in the form of inversion-symmetric *magnetic Weyl semimetals* [71–73].

At the level of the momentum-space Hamiltonian, inversion symmetry imposes the constraint

$$\mathcal{H}(\mathbf{k}) = U_{\mathcal{I}} \mathcal{H}(-\mathbf{k}) U_{\mathcal{I}}^{-1}. \quad (44)$$

Note that this symmetry has an action in momentum space that is similar to time reversal symmetry, the key difference being that the latter includes an anti-unitary rather than unitary conjugation. Importantly, inversion symmetry relates the same momenta on the Brillouin zone  $\mathbb{T}^3$  to each other; in particular, it induces the same set of eight fixed points, referred to as the time-reversal invariant momenta (TRIM). As explained in Sec. 3, the fixed points resulting from a non-free symmetry action need to be treated with additional scrutiny in the corresponding (co)homology description. For example, the classification of time-reversal symmetric Weyl semimetals in Ref. [47] relies on the use of equivariant homology *excluding* the TRIM, and twisted equivariant cohomology *relative to* the TRIM. Here, the twist in the cohomology group and treatment of the TRIM are based on precise arguments related to the classification of special equivariant vector bundle structures over the Brillouin zone [48]. As noted in Sec. 3, the twist in cohomology agrees in particular with the fact that each Weyl node has a symmetric partner of the same chirality.

For inversion symmetry, however, the symmetric partners of Weyl nodes instead have the opposite chirality, due to its unitary orientation-reversing nature. As such, the (co)homology classification of inversion-symmetric Weyl semimetals should rely on some form of twisted equivariant homology and ordinary equivariant cohomology. What remains is to find the correct treatment of the behaviour around the TRIM, which is qualitatively very different from the

time-reversal symmetric case: since a symmetric pair of Weyl nodes has opposite charges, they may be brought together and annihilated at any of the TRIM. This leads to the possibility of a configuration with two Weyl points in the Brillouin torus, connected by a Dirac string running through one of the TRIM; such a configuration is impossible in a time-reversal symmetric Weyl semimetal, which must host at least four Weyl points [6]. In principle, similarly rigorous arguments based on vector bundle classification can be constructed for a proper treatment of these fixed points; while such a description is certainly desirable in its own right, it is beyond the scope of the present work. Instead, we will demonstrate that the complete (co)homology description can be equally well obtained from a heuristic argument based on the aforementioned behaviour of Weyl points and Dirac strings at the TRIM.

The idea is as follows: in all of the cases studied above, the free action of the symmetry group  $G$  ensures that the fundamental domain takes on the topology of  $\mathbb{T}^3/G$  – for example,  $K^2 \times S^1 \cong \mathbb{T}^3/\mathbb{Z}_2$ , where  $\mathbb{Z}_2$  represents the single glide symmetry. This allows the equivariant (co)homology on  $\mathbb{T}^3$  to be reduced to ordinary (co)homology on the quotient space. Under the  $\mathbb{Z}_2$  inversion symmetry, the fundamental domain  $M$  “almost” has the topology of  $\mathbb{T}^3/\mathbb{Z}_2$ ; that is, all momenta in  $M$  act like the quotient of two points on the torus, except the eight TRIM. In light of this, Dirac strings in  $M$  that do not interact with the TRIM essentially act like elements of the usual (non-equivariant) twisted homology group  $H_1(M, W; \tilde{\mathbb{Z}})$ , where  $W$  is the set of Weyl points in  $M$ . Crucially, the aforementioned annihilation of one of the TRIM creates what seems from the perspective of  $M$  to be a Dirac string which terminates at the TRIM; this argument is illustrated in detail in Fig. 9. Recalling that homology relative to the set of Weyl points  $W$  encodes the fact that Dirac strings are allowed to terminate at these points, this leads us to propose that the correct classification in the case of inversion symmetry is given by twisted homology on  $M$  relative to the TRIM. This leads to the following ansatz for the exact twisted homology sequence:

$$\begin{aligned} 0 \rightarrow H_1(M, \text{TRIM}; \tilde{\mathbb{Z}}) &\rightarrow H_1(M, W \cup \text{TRIM}; \tilde{\mathbb{Z}}) \\ &\xrightarrow{\partial} H_0(W; \tilde{\mathbb{Z}}) \rightarrow H_0(M, \text{TRIM}; \tilde{\mathbb{Z}}) \rightarrow 0. \end{aligned} \quad (45)$$

Lefschetz duality ensures that there is a corresponding Mayer–Vietoris sequence in ordinary cohomology *excluding* the TRIM, which reads

$$\begin{aligned} 0 \rightarrow H^2(M \setminus \text{TRIM}) &\rightarrow H^2(M \setminus W \cup \text{TRIM}) \\ &\rightarrow \bigoplus_{w \in W} H^2(S_w^2) \rightarrow H^3(M \setminus \text{TRIM}) \rightarrow 0. \end{aligned} \quad (46)$$

Incidentally, the exclusion of the TRIM from these cohomology groups ensures that they are once again completely equivalent to equivariant cohomology on  $\mathbb{T}^3 \setminus \text{TRIM}$ , so that the sequence above may also be conceptualised in those terms.

Explicit calculation of this sequence is somewhat more involved than in the previously discussed cases, since  $M \setminus \text{TRIM}$  is non-compact and does not immediately admit a cell structure. To remedy this, a deformation retraction can be performed onto a suitable 2-skeleton; that is, the eight holes corresponding to the TRIM can be “grown” while maintaining the correct boundary identifications, until only a set of intersecting two-dimensional surfaces remains. This results in a complicated cell structure, on which the necessary cellular homology calculations are aided by computational tools such as the Smith normal form [74]. Going through these calculations yields the following explicit expression for the Mayer–Vietoris sequence in Eq. (46):

$$0 \rightarrow \mathbb{Z}^3 \oplus \mathbb{Z}_2^4 \rightarrow \mathbb{Z}^3 \oplus \mathbb{Z}_2^4 \oplus \mathbb{Z}^r \rightarrow \mathbb{Z}^r \rightarrow 0 \rightarrow 0, \quad (47)$$

where  $r$  denotes the number of Weyl points in the fundamental domain, i.e. the number of symmetric pairs of Weyl nodes on the torus.

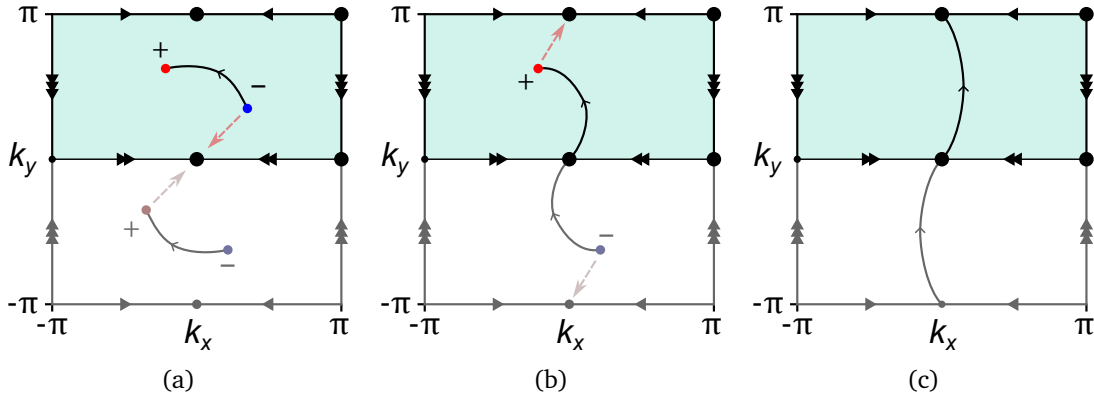


Figure 9: Illustration of a two-dimensional slice of the Brillouin torus at  $k_z = 0$ , with a choice of fundamental domain  $M$  highlighted in teal. The TRIM are indicated by bold black dots, and arrows indicate the correct boundary identifications on  $M$ . Starting with a basic Dirac string connecting two Weyl points in  $M$ , a series of Weyl point annihilation is played out on the torus, while the apparent topology of (twisted) Dirac strings and loops is studied in isolation within the fundamental domain; the complementary area is greyed out as a reminder of this. (a) The Dirac string contained within the fundamental domain first appears similar to an element of  $H_1(M, W; \mathbb{Z})$ . From this initial position, the negative Weyl point and its symmetric partner are brought together along the dashed arrows. (b) Eventually, these two Weyl points are annihilated at the TRIM at  $\mathbf{k} = 0$ . From the perspective of the fundamental domain, it seems as though the negative Weyl point is absorbed by the TRIM. Consequently, the Dirac string appears to be bounded by this TRIM as well as at the remaining Weyl point; that is, a Dirac string on  $M$  more properly acts as an element of  $H_1(M, W \cup \text{TRIM}; \mathbb{Z})$ . Note that this is still a valid description for panel (a), since the Dirac string depicted there terminates at  $W \subset (W \cup \text{TRIM})$ . (c) Annihilating the remaining two Weyl points at the TRIM at  $\mathbf{k} = (0, \pm\pi, 0)$  results in a Dirac loop that, from the perspective of the fundamental domain, runs between two different TRIM; in other words, Dirac loops act like elements of  $H_1(M, \text{TRIM}; \mathbb{Z})$  in this system.

The sequence in Eq. (47) has one feature which immediately stands out: the total charge group appearing on the right is now the trivial zero group, whereas this group is  $\mathbb{Z}$  on the basic torus and  $\mathbb{Z}_2$  on each non-orientable Brillouin zone discussed previously. Physically, this means that the notion of charge cancellation is completely absent on the fundamental domain – here, the total chirality can take on any value. Intuitively speaking, this relates to the fact that the system admits configurations such as those illustrated in Fig. 9(b), where the fundamental domain hosts a single Weyl point of unit charge. It should be emphasised that the lack of charge cancellation on the fundamental domain is not an indication of any physical anomalies, just as in the case of  $K^2 \times S^1$ . Instead, it should be understood in terms of the Weyl points being related to their own charge cancelling partner through the symmetry.

The  $\mathbb{Z}^3 \oplus \mathbb{Z}_2^4$  group of insulating invariants appearing on the left side of Eq. (47) is most readily interpreted in terms of twisted Dirac loops, as was done for the glide symmetry in Sec. 4.2. We take Fig. 9(c) as starting point, where an inversion-symmetric twisted Dirac loop is depicted which runs through the two TRIM at  $\mathbf{k} = (0, 0, 0)$  and  $\mathbf{k} = (0, \pi, 0)$  along the positive  $k_y$ -direction; we will denote this loop by  $\ell_{0y0}$ . This loop cannot be removed from the two TRIM it crosses by symmetry-preserving continuous deformations, meaning it is topologically distinct from the three other possible Dirac loops  $\ell_{0y\pi}$ ,  $\ell_{\pi y0}$ , and  $\ell_{\pi y\pi}$  that run through two TRIM in the positive  $k_y$ -direction. Taken together with the four similarly defined

loops in the  $k_x$  and  $k_z$ -directions, there are a total of 12 such basic twisted Dirac loops. The twisted homology classes of these 12 loops generate the  $\mathbb{Z}^3 \oplus \mathbb{Z}_2^4$  group; this can be understood more precisely by studying the ways in which they can be detached from the TRIM points.

As an example of this, consider a situation in which two loops of the form  $\ell_{0y0}$  are present at the same time. If two such loops are present, they can be detached from  $(0,0,0)$  and  $(0,\pi,0)$  in a symmetry-preserving fashion; this is illustrated in Fig. 10 (a). After moving the

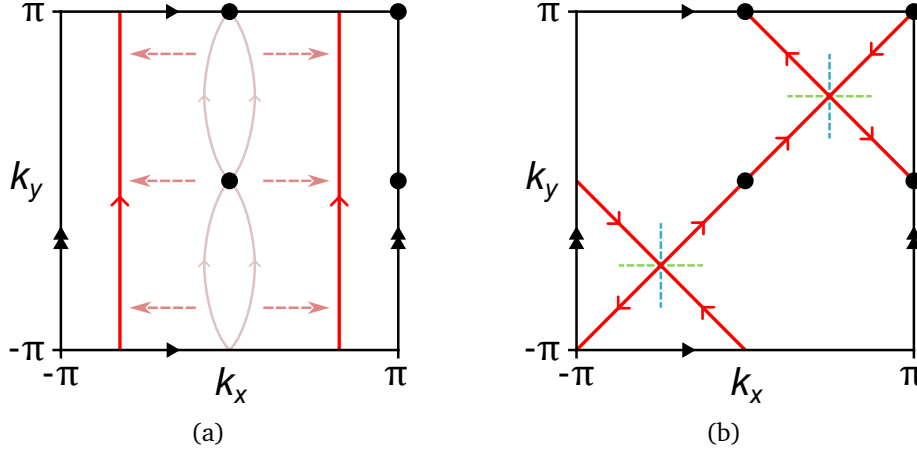


Figure 10: (a) Two copies of  $\ell_{0y0}$  can be moved apart in opposite directions while respecting inversion symmetry. Moving the loops even further apart makes them intersect the TRIM at  $k_x = \pi$  simultaneously, proving that in terms of twisted homology classes,  $2[\ell_{0y0}] = 2[\ell_{\pi y0}]$ . (b) Intermediate state between  $\ell_{0y0} - \ell_{\pi y0}$  and  $\ell_{x00} - \ell_{x\pi0}$ . Detaching the intersections along the vertical blue dashed lines (as though cutting them with scissors) yields  $\ell_{0y0} - \ell_{\pi y0}$ , whereas cutting along the horizontal green lines gives  $\ell_{x00} - \ell_{x\pi0}$ ; here, the negative sign in both expressions is reflected in the fact that the corresponding loops run in the negative coordinate direction.

two loops apart, they can instead be made to simultaneously intersect the TRIM at  $(\pi,0,0)$  and  $(\pi,\pi,0)$ , meaning that they have been deformed into two copies of  $\ell_{\pi y0}$ . As a result, the twisted homology classes  $[\ell_{0y0}]$  and  $[\ell_{\pi y0}]$  are interdependent, and therefore unable to generate separate  $\mathbb{Z}$  invariants; this is precisely why only three factors of  $\mathbb{Z}$  appear in the invariant group, corresponding to the three coordinate directions. Meanwhile, the difference between these two classes is necessarily a  $\mathbb{Z}_2$  invariant since

$$2[\ell_{0y0}] = 2[\ell_{\pi y0}] \implies 2[\ell_{0y0} - \ell_{\pi y0}] = 0. \quad (48)$$

Furthermore, a simple argument depicted in Fig. 10(b) shows that this difference  $[\ell_{0y0} - \ell_{\pi y0}]$  is equivalent to the difference  $[\ell_{x00} - \ell_{x\pi0}]$  of two loops running in the positive  $x$  direction.

Functionally similar arguments give rise to additional relations between the basic twisted Dirac loops. All in all, we conclude that the insulating invariant group  $\mathbb{Z}^3 \oplus \mathbb{Z}_2^4$  admits a basis of three  $\mathbb{Z}$  generators given by

$$v_x := [\ell_{x00}], \quad v_y := [\ell_{0y0}], \quad v_z := [\ell_{00z}], \quad (49)$$

along with four  $\mathbb{Z}_2$  generators given by

$$\begin{aligned} v_{xy} &:= [\ell_{x00} - \ell_{x\pi0}] = [\ell_{0y0} - \ell_{\pi y0}], & v_{xyz} &:= [\ell_{x00} - \ell_{x\pi0} - \ell_{x0\pi} + \ell_{x\pi\pi}] \\ v_{yz} &:= [\ell_{0y0} - \ell_{0y\pi}] = [\ell_{00z} - \ell_{0\pi z}], & &= [\ell_{0y0} - \ell_{\pi y0} - \ell_{0y\pi} + \ell_{\pi y\pi}] \\ v_{xz} &:= [\ell_{00z} - \ell_{\pi 0z}] = [\ell_{x00} - \ell_{x0\pi}], & &= [\ell_{00z} - \ell_{\pi 0z} - \ell_{0\pi z} + \ell_{\pi\pi z}], \end{aligned} \quad (50)$$



all together generating the full topological description of the insulating phases.

As before, the semimetal invariants in the group  $\mathbb{Z}^3 \oplus \mathbb{Z}_2^4 \oplus \mathbb{Z}^k$  can be fully understood in terms of this insulating description, in the sense that the creation and annihilation of pairs of Weyl nodes along the loops discussed above mediates phase transitions between different insulating invariants.

We finish this section by noting that our description in terms of twisted Dirac loops agrees well with previously established conclusions in the context of inversion-symmetric insulators. In particular, a many-band description of such insulators is given in Ref. [75], in terms of three  $\mathbb{Z}$ -valued Chern numbers and eight other  $\mathbb{Z}$  invariants based on eigenvalues of the inversion symmetry at each of the eight TRIM. In the present two-band setting, the latter eight  $\mathbb{Z}$  invariants are reduced to  $\mathbb{Z}_2$  invariants, corresponding to the  $\mathbb{Z}_2$  symmetry eigenvalue on the occupied band at each TRIM. These eight are further reduced to the four independent  $\mathbb{Z}_2$  factors appearing in the group  $\mathbb{Z}^3 \oplus \mathbb{Z}_2^4$  by imposing physical constraints on these occupied states. Concretely, the eigenvalues  $\zeta \in \mathbb{Z}_2 := \{\pm 1\}$  are bound to satisfy

$$\prod_{\kappa \in \text{TRIM}} \zeta(\kappa) = 1, \quad \prod_{\kappa \in \text{TRIM}_{k_i=0}} \zeta(\kappa) = (-1)^{C_i} \quad (51)$$

for insulating states; here  $\text{TRIM}_{k_i=0}$  denotes the four TRIM lying in the  $k_i = 0$  plane for any  $i \in \{x, y, z\}$ , and  $C_i$  is the corresponding Chern number as calculated in Eq. (7). These  $\mathbb{Z}_2$  eigenvalues have a precise interpretation in terms of the homology framework given above: the eigenvalue at any given TRIM is  $-1$  precisely when a twisted Dirac loop or string passes through that point.

## 6 Summary, discussion and outlook

### 6.1 Summary

In this work we have provided a coordinate-free description classifying the topology of Weyl semimetals with non-orientable Brillouin zones arising from orientation-reversing symmetries. We show that the topological features induced by such symmetries can be understood within a framework employing certain exact sequences in (co)homology. Rather than admitting a description in terms of ordinary homology and cohomology groups, the loss of orientability breaks conventional Poincaré duality, which invalidates the standard correspondence between the cohomology and homology descriptions. This Poincaré duality is restored by introducing a twist in either the homology or the cohomology groups. Through a straightforward argument involving the impact of orientation reversal on the Weyl points and their concomitant Dirac strings, we show that the correct choice of this twist can be arrived at by studying pairs of Weyl points related by orientation-reversing symmetry: opposite chiralities in such a pair indicate the use of twisted homology, whereas pairs of the same chirality indicate that the cohomology is twisted.

This framework is then applied to the case of a  $K^2 \times S^1$  Brillouin zone arising from a single momentum-space glide symmetry. Identifying the correct Mayer–Vietoris sequence in ordinary cohomology groups and its dual sequence in twisted homology, we provide a derivation of the mod 2 charge cancellation theorem existing in this context, and classify the accompanying topological invariants for the insulating and semimetallic phases. Importantly, the coordinate-free description demonstrates that any apparent non-zero net chirality in the  $K^2 \times S^1$  fundamental domain is unphysical in nature, being dependent on an arbitrary choice of basis for the group of local charges; physically, this corresponds to a given parametrisation of the fundamental domain. The topological invariants of the system are interpreted both in terms

of integration of (cohomological) differential forms, and in terms of (homological) twisted Dirac strings, and the corresponding surface states on  $K^2$ -like surfaces are derived through the introduction of a projection map and its corresponding pushforward on homology.

The classification scheme is then applied in three additional contexts. First, we complete the classification of all possible three-dimensional non-orientable Brillouin zones, by studying all orientation-reversing space group symmetries with a free action. Four such topologies are found to exist in total: the previously studied  $K^2 \times S^1$  arising from the space group  $Pc$ , and three other topologies related to the groups  $Cc$ ,  $Pca2_1$ , and  $Pna2_1$ . In all cases, similar mod 2 charge cancellation conditions are derived, but the insulating and semimetallic invariants are shown to differ between these groups. Second, the exact sequences on  $K^2$ -like surfaces are related to non-Hermitian systems, and used to elucidate the mod 2 charge cancellation for exceptional points in non-Hermitian two-band systems. Finally, we use heuristic arguments to provide a topological classification of inversion-symmetric Weyl semimetals in terms of twisted homology groups relative to the TRIM points. This reproduces the known insulating invariants and reframes them in terms of twisted Dirac loops, while at the same time providing a sensible understanding of the topology of the Weyl points; together, this allows the full semimetallic topology to be readily understood.

## 6.2 Discussion and outlook

The topological classification scheme in terms of (co)homology groups developed in this work not only serves as a fundamental theoretical framework encoding theoretical aspects of topological invariants and their origins, but also proves to be remarkably powerful from the perspective of physical interpretation. The complete overview it provides of all the rules and consequences related to Weyl point annihilation and creation is significant in its own right, but arguably the most compelling physical implication of the invariant groups arises in the classification of the insulating phases of systems subject to inversion symmetry. In this context, it is shown in Ref. [75] that many-band inversion-symmetric topological insulators can be divided into 16 different classes distinguishable by their transport properties for any given Chern vector. This might be explained precisely by the  $\mathbb{Z}^3 \oplus \mathbb{Z}_2^4$  structure of the invariant group that we find in the two-band homology treatment: the Chern number fixes an element of the first factor  $\mathbb{Z}^3$ , while the remaining  $\mathbb{Z}_2^4$  factor has precisely  $2^4 = 16$  elements. We have not made this correspondence precise, but in general it should not be surprising that transport properties are well described by two-band models: such models focus solely on dispersion at the Fermi level by isolating the valence and conduction bands. If the correspondence does indeed turn out to be exact, this highlights the great potential of two-band descriptions in predicting physical features which are also present in multi-band models.

One of the principal aims of this work has been to clarify the physical interpretation of the mod 2 charge cancellation theorem present on non-orientable Brillouin zones. In this context, the insights gained in this work give rise to a minor conceptual analogy between the apparent non-zero chirality appearing on the fundamental domain on one hand, and ghost fields in quantum field theory on the other hand. This can be understood as follows: in quantum field theory, ghost fields arise when local gauge degrees of freedom are fixed in order to make certain integrals tractable. These fields come with their own respective particles, which may appear in valid Feynman diagrams; however, a choice of gauge may always be made which removes the ghost field completely, so that these ghost particles are purely mathematical in nature and cannot be observed physically. Similarly, the Weyl point charges on a non-orientable Brillouin zone are subject to a local degree of freedom relating to the local choice of orientation at each point – that is, a basis can be freely chosen for the group of these charges. Fixing such a choice may give rise to a net non-zero chirality, seemingly resulting in a chiral anomaly; however, just as in the case of ghost fields, a choice can instead be made which makes this net charge

disappear, so that it cannot be assigned physical meaning. This can also be framed in somewhat more field-theoretic terms: the tangent bundle of a non-orientable manifold does not admit a spin structure, so that an effective field theory of Weyl spinors cannot naturally be described in terms of an abstract tangent vector field on these manifolds. The formulation of such an effective field theory will thus necessarily depend on an arbitrary choice of coordinates; this similarly leads to apparent chiral anomalies which may be resolved by a change of coordinates, prohibiting any phenomenological consequences.

Importantly, this lack of phenomenological consequences does not necessarily mean that the classification scheme developed in this work is of no experimental relevance. On the contrary, it sheds light on and provides important knowledge regarding already conducted experiments [49], as well as any potential future experiments. In particular, the homology interpretation of Dirac strings and Fermi arcs provide a solid mathematical and physical understanding of the global structure of systems such as the one studied in Ref. [49]. In this regard, we emphasise that we do not question the validity of the actual measurements performed in that work, but rather want to convey the opinion that observations of this nature should be accompanied by complementary measurements using different parametrisations of the fundamental domain. One interesting potential avenue for such experiments lies in a fully three-dimensional realisation of non-orientable Weyl semimetals in the context of three-dimensional acoustic crystals. Non-symmorphic momentum-space symmetries have been successfully studied in this context [52], as have Weyl semimetals [76–78]; combining these two aspects would allow many of the physical properties of the systems studied in this work to be probed directly.

It should also be mentioned that circumventions of the Nielsen–Ninomiya theorem have been studied somewhat extensively in other setups, including Floquet systems [79–81] and flux-biased Weyl superconductors [82], where the system setups seemingly result in observable phenomena, such as equilibrium chiral magnetic effects sourced by a net chiral anomaly [83]. Whether or not these systems are even remotely related to the notion of non-orientable Brillouin zones, or how these are to be treated in terms of a classification scheme similar to the one developed in this work, comprises an interesting question to be answered in future research projects.

On a more theoretically fundamental level, there are several open questions that deserve to be addressed in future works. One immediate such question originating from the current work concerns the physics of additional surface states on non-orientable Brillouin zones. In this work, the surface states obtained by projecting out the periodic  $S^1$  factor of  $K^2 \times S^1$  are studied, but potential topological surface states are also bound to exist upon projection along the other two coordinate directions. These other projections interact with the glide symmetry in a non-trivial way, and as such they do not necessarily preserve its orientation-reversing properties. This leads us to believe that such surface states may need to be classified using a more involved and modified (co)homology description. An additional avenue for research lies in the formulation of similar classifications for systems subject to other symmetries, both with free and non-free actions. In particular, venturing into the realm of symmetries with non-free actions opens the possibility to provide similar (co)homology descriptions of systems subject to two mutually orthogonal glide symmetries, whose fundamental domains share some topological properties with the real projective space  $\mathbb{R}P^2$ , or in three dimensions, its direct product with the circle  $\mathbb{R}P^2 \times S^1$  – notably, the presence of fixed momenta under this symmetry ensures that these spaces do not act as proper Brillouin zones. Such fundamental domains are studied in Refs. [49, 54], indicating their immediate interest in the community. To the knowledge of the authors, descriptions in the specific terms of dual exact sequences for homology and cohomology exist for systems without symmetries [37, 38] (a description that can be directly carried over to systems subject to chiral symmetry), and systems subject to time reversal sym-

metry [47]. Hermitian systems subject to the simultaneous combination of parity and time reversal symmetry, resulting in so-called knotted semimetals, have also been studied in this context, although a satisfactory classification scheme remains elusive to date [84]. It should be noted that descriptions of many of these symmetries have been provided in the context of K-theory, which is a generalised cohomology theory; notably, Ref. [46] provides a K-theoretic classification of systems subject to all 230 space groups, including semimetallic information. However, these works generally do not exploit the relation between local and global topology which is contained in the Mayer–Vietoris sequences studied here, nor the Poincaré duality giving rise to dual homology descriptions, while both of these aspects prove to contribute much intuitive physical insight. In principle, these features can also be reproduced in the K-theoretic setting; in particular, there is a notion of twisted Poincaré duality in this context [85]. One major advantage of this K-theoretic point of view is that it generalises well to non-Abelian descriptions via the study of non-commutative geometry, potentially enabling the study of features such as non-Abelian spectral braiding in non-Hermitian systems.

In general, there is vast potential for expansion into this non-Hermitian regime. As previously mentioned, the case of two-dimensional glide-symmetric non-Hermitian systems and mod 2 charge cancellations of exceptional points has recently been studied in Refs. [54, 55]. One interesting observation made in Ref. [54] pertains to specific kinds of non-Abelian phase transitions related to the so-called rebasing operation. Such transitions are sensitive to similar fundamental domain reparametrisations as those discussed in this work, and as such may not represent true transitions between distinct topological phases of the system. Possibly, the homotopy description of this phenomenon is better understood in terms of fundamental groupoids rather than fundamental groups, in which such rebasing operations induce isomorphisms between fundamental groups. A proper (co)homology treatment of this behaviour is confounded by its non-Abelian nature, although it may be that it is well-described by the aforementioned extensions to non-commutative geometry.

## 7 Conclusion

The interplay between condensed matter physics and topology has revolutionised modern physics research in recent decades, paving the way towards state-of-the-art semiconductor devices and notable achievements in quantum information – with semimetallic and superconducting implementations marking future milestones. Many key material properties are readily described by the interplay between the valence and conduction bands, thus offering a compelling explanation even within the theory of two-band models. Even so, fundamental topological classifications of these properties stemming from the framework of algebraic topology are surprisingly rare, despite their potential in providing not only a fundamental mathematical understanding of their origin, but also their physical interpretation.

Our work highlights how the complete understanding of topological semimetals and insulators benefits from such a fundamental topological description. This is exemplified through the use of twisted (co)homology for the classification of semimetals subject to orientation-reversing symmetries, including space group symmetries with free actions and inversion symmetry. In particular, our classification scheme provides a proper physical understanding of the accompanying modified cancellation theorems, and remedies the corresponding interpretation of net non-zero chiralities and chiral anomalies in these systems. We also show that the classification scheme can be extended further to the non-Hermitian regime, giving it further relevance in the context of dissipative and open quantum systems and paving the way towards an increased physical and mathematical understanding of systems relevant in a wide range of different areas of today’s physics research.

## Acknowledgements

Both authors express their gratitude to Cristiane Morais Smith for extensive discussions and supervision throughout the project. Scientific and social discussions with Diego Felipe Muñoz-Arboleda, Lumen Eek, Anouar Moustaj, David Santiago Quevedo Vega, and Robin Verstraten are further acknowledged. MS is supported by the Swedish Research Council (VR) under grant number 2024.00272.

## References

- [1] K. von Klitzing, *New Method for High-Accuracy Determination of the Fine-Structure Constant Based on Quantized Hall Resistance*, Phys. Rev. Lett. **45**, 494 (1980), doi:[10.1103/PhysRevLett.45.494](https://doi.org/10.1103/PhysRevLett.45.494).
- [2] J.C. Budich and B. Trauzettel, *From the adiabatic theorem of quantum mechanics to topological states of matter*, Phys. Status Solidi **7**, 109 (2013), doi:[10.1002/pssr.201206416](https://doi.org/10.1002/pssr.201206416)
- [3] M.Z. Hasan and C.L. Kane, *Colloquium: Topological insulators*, Rev. Mod. Phys. **82**, 3045 (2010), doi:[10.1103/RevModPhys.82.3045](https://doi.org/10.1103/RevModPhys.82.3045).
- [4] X.-L. Qi and S.-C. Zhang, *Topological insulators and superconductors*, Rev. Mod. Phys. **83**, 1057 (2011), doi:[10.1103/RevModPhys.83.1057](https://doi.org/10.1103/RevModPhys.83.1057).
- [5] M.O. Goerbig, *Electronic properties of graphene in a strong magnetic field*, Rev. Mod. Phys. **83**, 1193 (2011), doi:[10.1103/RevModPhys.83.1193](https://doi.org/10.1103/RevModPhys.83.1193).
- [6] N.P. Armitage, E.J. Mele, and A. Vishwanath, *Weyl and Dirac semimetals in three-dimensional solids*, Rev. Mod. Phys. **90**, 015001 (2018), doi:[10.1103/RevModPhys.90.015001](https://doi.org/10.1103/RevModPhys.90.015001).
- [7] P. Hosur, and X. Qi *Recent developments in transport phenomena in Weyl semimetals*, Comptes Rendus Physique **14**, 9-10, (2013), doi:[10.1016/j.crhy.2013.10.010](https://doi.org/10.1016/j.crhy.2013.10.010).
- [8] S.-Y. Xu, I. Belopolski, N. Alidoust, M. Neupane, G. Bian, C. Zhang, R. Sankar, G. Chang, Z. Yuan, C.-C. Lee, S.-M. Huang, H. Zheng, J. Ma, D. S. Sanchez, B. Wang, A. Bansil, F. Chou, P.P. Shibayev, H. Lin, S. Jia, and M.Z. Hasan, *Discovery of a Weyl fermion semimetal and topological Fermi arcs*, Science **349**, 613 (2015), doi:[10.1126/science.aaa9297](https://doi.org/10.1126/science.aaa9297).
- [9] B.Q. Lv, H.M. Weng, B.B. Fu, X.P. Wang, H. Miao, J. Ma, P. Richard, X.C. Huang, L.X. Zhao, G.F. Chen, Z. Fang, X. Dai, T. Qian, and H. Ding, *Experimental Discovery of Weyl Semimetal TaAs*, Phys. Rev. X **5**, 031013 (2015), doi:[10.1103/PhysRevX.5.031013](https://doi.org/10.1103/PhysRevX.5.031013).
- [10] S.-Y. Xu, I. Belopolski, D. S. Sanchez, C. Zhang, G. Chang, C. Guo, G. Bian, Z. Yuan, H. Lu, and M. Z. Hasan, *Experimental discovery of a topological Weyl semimetal state in TaP*, Sci. Adv. **1**, e1501092 (2015), doi:[10.1126/sciadv.1501092](https://doi.org/10.1126/sciadv.1501092).
- [11] N. Nagaosa, and T. Morimoto, *Concept of Quantum Geometry in Optoelectronic Processes in Solids: Application to Solar Cells*, Advanced Materials **29**, 1603345 (2017), doi:[10.1002/adma.201603345](https://doi.org/10.1002/adma.201603345).
- [12] J. Liu, F. Xia, D. Xiao, F.J. García de Abajo, and D. Sun, *Semimetals for high-performance photodetection*, Nat. Mater. **19**, 830-837 (2020), doi:[10.1038/s41563-020-0715-7](https://doi.org/10.1038/s41563-020-0715-7).



- [13] Z.-H. Chen, Z.-Y. Fang, T.-X. Liu, H.-J. Duan, M. Yang, M.-X. Deng, and R.-Q. Wang, *Quantum oscillation of the circular photogalvanic effect in Weyl semimetals under strong magnetic fields*, Phys. Rev. B **110**, 115149 (2024), doi:[10.1103/PhysRevB.110.115149](https://doi.org/10.1103/PhysRevB.110.115149).
- [14] H. Weyl, *Elektron und Gravitation. I*, Z. Physik **56**, 330 (1929), doi:[10.1007/BF01339504](https://doi.org/10.1007/BF01339504).
- [15] L. Lu, Z. Wang, D. Ye, L. Ran, L. Fu, J.D. Joannopoulos, and M. Soljačić, *Experimental observation of Weyl points*, Science **349**, 6248, 622-624 (2015), doi:[10.1126/science.aaa9273](https://doi.org/10.1126/science.aaa9273).
- [16] G.E. Volovik, *Black hole and hawking radiation by type-II Weyl fermions*, JETP Letters **104**, pages645–648 (2016), doi:[10.1134/S0021364016210050](https://doi.org/10.1134/S0021364016210050).
- [17] M.A. Zubkov, *Analogies between the Black Hole Interior and the Type II Weyl Semimetals*, Universe **4**, 135 (2018), doi:[10.3390/universe4120135](https://doi.org/10.3390/universe4120135).
- [18] G.E. Volovik, and K. Zhang, *Lifshitz Transitions, Type-II Dirac and Weyl Fermions, Event Horizon and All That*, J. Low Temp. Phys. **189**, (2017), doi:[10.1007/s10909-017-1817-8](https://doi.org/10.1007/s10909-017-1817-8).
- [19] M.A. Zubkov, *The black hole interior and the type II Weyl fermions*, Mod. Phys. Lett. A Vol. **33**, 1850047 (2018), doi:[10.1142/S0217732318500475](https://doi.org/10.1142/S0217732318500475).
- [20] H. Liu, J.-T. Sun, H. Huang, F. Liu, and S. Meng, *Fermionic analogue of black hole radiation with a super high Hawking temperature*, Chin. Phys. Lett., **37**, 6, 067101 (2020), doi:[10.1088/0256-307X/37/6/067101](https://doi.org/10.1088/0256-307X/37/6/067101).
- [21] Y. Kedem, E.J. Bergholtz, and F. Wilczek *Black and White Holes at Matetrial Junctions*, Phys. Rev. Research **2**, 043285 (2020), doi:[10.1103/PhysRevResearch.2.043285](https://doi.org/10.1103/PhysRevResearch.2.043285).
- [22] J. Nissinen, G.E. Volovik, *Type-III and IV interacting Weyl points*, Jetp Lett. **105**, 447–452 (2017), doi:[10.1134/S0021364017070013](https://doi.org/10.1134/S0021364017070013).
- [23] C.-L. Zhang, S.-Y. Xu, I. Belopolski, Z. Yuan, Z. Lin, B. Tong, G. Bian, N. Alidoust, C.-C. Lee, S.-M. Huang, T.-R. Chang, G. Chang, C.-H. Hsu, H.-R. Jeng, M. Neupance, D.S. Sanchez, H. Zheng, J. Wang, H. Lin, C. Zhang, H.-Z. Lu, S.-Q. Shen, T. Neupert, M.Z. Hasan, and S. Jia, *Signatures of the Adler–Bell–Jackiw chiral anomaly in a Weyl fermion semimetal*, Nature Comms. **7** 10735 (2016), doi:[10.1038/ncomms10735](https://doi.org/10.1038/ncomms10735).
- [24] C.-X. Liu, P. Ye, and X.-L. Qi, *Chiral gauge field and axial anomaly in a Weyl semimetal*, Phys. Rev. B **87**, 235306 (2015), doi:[10.1103/PhysRevB.87.235306](https://doi.org/10.1103/PhysRevB.87.235306).
- [25] D.T. Son, and N. Yamamoto, *Berry Curvature, Triangle Anomalies, and the Chiral Magnetic Effect in Fermi Liquids*, Phys. Rev. Lett. **109**, 181602 (2012), doi:[10.1103/PhysRevLett.109.181602](https://doi.org/10.1103/PhysRevLett.109.181602).
- [26] A.G. Grushin, *Consequences of a condensed matter realization of Lorentz-violating QED in Weyl semi-metals*, Phys. Rev. D **86**, 045001 (2012), doi:[10.1103/PhysRevD.86.045001](https://doi.org/10.1103/PhysRevD.86.045001).
- [27] A.A. Zyuzin and A.A. Burkov, *Topological response in Weyl semimetals and the chiral anomaly*, Phys. Rev. B **86**, 115133 (2012), doi:[10.1103/PhysRevB.86.115133](https://doi.org/10.1103/PhysRevB.86.115133).
- [28] P. Goswami and S. Tewari, *Axionic field theory of (3+1)-dimensional Weyl semimetals*, Phys. Rev. B **88**, 245107 (2013), doi:[10.1103/PhysRevB.88.245107](https://doi.org/10.1103/PhysRevB.88.245107).



- [29] S.A. Parameswaran, T. Grover, D.A. Abanin, D.A. Pesin, and A. Vishwanath, *Probing the Chiral Anomaly with Nonlocal Transport in Three-Dimensional Topological Semimetals*, Phys. Rev. X **4**, 031035 (2014), doi:[10.1103/physrevx.4.031035](https://doi.org/10.1103/physrevx.4.031035).
- [30] J. Klier, I.V. Gornyi, and A.D. Mirlin, *Transversal magnetoresistance in Weyl semimetals*, Phys. Rev. B **92**, 205113 (2015), doi:[10.1103/physrevb.92.205113](https://doi.org/10.1103/physrevb.92.205113).
- [31] J. Klier, I.V. Gornyi, and A.D. Mirlin, *Transversal magnetoresistance and Shubnikov–de Haas oscillations in Weyl semimetals*, Phys. Rev. B **96**, 214209 (2017), doi:[10.1103/PhysRevB.96.214209](https://doi.org/10.1103/PhysRevB.96.214209).
- [32] J. Behrends, F.K. Kunst, and B. Sbierski, *Transversal magnetotransport in Weyl semimetals: Exact numerical approach*, Phys. Rev. B **97**, 064203 (2018), doi:[10.1103/PhysRevB.97.064203](https://doi.org/10.1103/PhysRevB.97.064203).
- [33] X. Huang, L. Zhao, Y. Long, P. Wang, D. Chen, Z. Yang, H. Liang, M. Xue, H. Weng, Z. Fang, X. Dai, and G. Chen, *Observation of the Chiral-Anomaly-Induced Negative Magnetoresistance in 3D Weyl Semimetal TaAs*, Phys. Rev. X **5**, 031023 (2015), doi:[10.1103/physrevx.5.031023](https://doi.org/10.1103/physrevx.5.031023).
- [34] H.B. Nielsen, M. Ninomiya, *Absence of neutrinos on a lattice: (I). Proof by homotopy theory*, Nuclear Physics B **185**, 1 20-40, (1981), doi:[10.1016/0550-3213\(81\)90361-8](https://doi.org/10.1016/0550-3213(81)90361-8).
- [35] H.B. Nielsen, M. Ninomiya, *Absence of neutrinos on a lattice: (II). Intuitive topological proof*, Nuclear Physics B **193**, 1 173-194, (1981), doi:[10.1016/0550-3213\(81\)90524-1](https://doi.org/10.1016/0550-3213(81)90524-1).
- [36] H.B. Nielsen, and M. Ninomiya, *The Adler-Bell-Jackiw anomaly and Weyl fermions in a crystal*, Phys. Lett. B **130**, 6, 389-396 (1983), doi:[10.1016/0370-2693\(83\)91529-0](https://doi.org/10.1016/0370-2693(83)91529-0).
- [37] V. Mathai, G.C. Thiang, *Differential Topology of Semimetals*, Commun. Math. Phys. **355**, 561–602 (2017), doi:[10.1007/s00220-017-2965-z](https://doi.org/10.1007/s00220-017-2965-z).
- [38] V. Mathai, G.C. Thiang, *Global topology of Weyl semimetals and Fermi arcs*, J. Phys. A: Math. Theor. **50** 11LT01 (2017), doi:[10.1088/1751-8121/aa59b2](https://doi.org/10.1088/1751-8121/aa59b2).
- [39] A. Altland, M.R. Zirnbauer, *Nonstandard symmetry classes in mesoscopic normal-superconducting hybrid structures*, Phys. Rev. B **55**, 1142 (1997), doi:[10.1103/PhysRevB.55.1142](https://doi.org/10.1103/PhysRevB.55.1142).
- [40] A.P. Schnyder, S. Ryu, A. Furusaki, and A.W.W. Ludwig, *Classification of topological insulators and superconductors in three spatial dimensions*, Phys. Rev. B **78**, 195125 (2008), doi:[10.1103/PhysRevB.78.195125](https://doi.org/10.1103/PhysRevB.78.195125).
- [41] A. Kitaev, *Periodic table for topological insulators and superconductors*, AIP Conf. Proc. **1134**, 22 (2009), doi:[10.1063/1.3149495](https://doi.org/10.1063/1.3149495).
- [42] S. Ryu, A.P. Schnyder, A. Furusaki, and A.W.W. Ludwig, *Topological insulators and superconductors: tenfold way and dimensional hierarchy*, New J. Phys. **12**, 065010 (2010), doi:[10.1088/1367-2630/12/6/065010](https://doi.org/10.1088/1367-2630/12/6/065010).
- [43] D.S. Freed, and G.W. Moore, *Twisted Equivariant Matter*, Ann. Henri Poincaré **14**, 1927–2023 (2013), doi:[10.1007/s00023-013-0236-x](https://doi.org/10.1007/s00023-013-0236-x).
- [44] G.C. Thiang, *On the K-Theoretic Classification of Topological Phases of Matter*, Ann. Henri Poincaré **17**, 757–794 (2016), doi:[10.1007/s00023-015-0418-9](https://doi.org/10.1007/s00023-015-0418-9)

- [45] K. Gomi, *Freed-Moore K-theory*, arXiv:1705.09134, doi:[10.48550/arXiv.1705.09134](https://doi.org/10.48550/arXiv.1705.09134).
- [46] K. Shiozaki, M. Sato, and K. Gomi, *Atiyah-Hirzebruch spectral sequence in band topology: General formalism and topological invariants for 230 space groups*, Phys. Rev. B **106**, 165103 (2022), doi:[10.1103/PhysRevB.106.165103](https://doi.org/10.1103/PhysRevB.106.165103).
- [47] G. C. Thiang, K. Sato, and K. Gomi, *Fu-Kane-Mele monopoles in semimetals*, Nucl. Phys. B **923** 107-125 (2017), doi:[10.1016/j.nuclphysb.2017.07.018](https://doi.org/10.1016/j.nuclphysb.2017.07.018).
- [48] G. De Nittis, and K. Gomi, *The cohomological nature of the Fu-Kane-Mele invariant*, Journal of Geometry and Physics **124**, 124-164 (2018), doi:[10.1016/j.geomphys.2017.10.007](https://doi.org/10.1016/j.geomphys.2017.10.007).
- [49] A.G. Fonseca, S. Vaidya, T. Christensen, M.C. Rechtsman, T.L. Hughes, and M. Soljačić, *Weyl Points on Nonorientable Manifolds*, Phys. Rev. Lett. **132**, 266601 (2024), doi:[10.1103/PhysRevLett.132.266601](https://doi.org/10.1103/PhysRevLett.132.266601).
- [50] Z.Y. Chen, S.A. Yang, Y.X. Zhao, *Brillouin Klein bottle from artificial gauge fields*, Nat. Commun. **13** 2215 (2022), doi:[10.1038/s41467-022-29953-7](https://doi.org/10.1038/s41467-022-29953-7).
- [51] Y.-L. Tao, M. Yan, M. Peng, Q. Wei, Z. Cui, S.A. Yang, G. Chen, and Y. Xu, *Higher-order Klein bottle topological insulator in three-dimensional acoustic crystals*, Phys. Rev. B **109**, 134107 (2024), doi:[10.1103/PhysRevB.109.134107](https://doi.org/10.1103/PhysRevB.109.134107).
- [52] Z. Zhu, L. Yang, J. Wu, Y. Meng, X. Xi, B. Yan, J. Chen, J. Lu, X. Huang, W. Deng, C. Shang, P.P. Shum, Y. Yang, H. Chen, K. Xiang, G.-G. Liu, Z. Liu, Z. Gao, *Brillouin Klein space and half-turn space in three-dimensional acoustic crystals*, Science Bulletin **69**, 13, 2050-2058 (2024), doi:[10.1016/j.scib.2024.05.003](https://doi.org/10.1016/j.scib.2024.05.003).
- [53] Y. Wang, C. Zhang, Z.Y. Chen, B. Liang, Y.X. Zhao, J. Cheng, *Chess-board Acoustic Crystals with Momentum-space Nonsymmorphic Symmetries*, arXiv:2305.07174, doi:[10.48550/arXiv.2305.07174](https://doi.org/10.48550/arXiv.2305.07174).
- [54] J.L.K. König, K. Yang, A.G. Fonseca, S. Vaidya, M. Soljačić, E.J. Bergholtz, *Exceptional Topology on Nonorientable Manifolds*, arXiv:2503.04889, doi:[10.48550/arXiv.2503.04889](https://doi.org/10.48550/arXiv.2503.04889).
- [55] W.B. Rui, Z.D. Wang, *Exceptional Non-Hermitian Topology Associated with Non-Toroidal Brillouin Zones*, Phys. Rev. B **112**, L041127 (2025), doi:[10.1103/h9c2-h3t7](https://doi.org/10.1103/h9c2-h3t7).
- [56] R. Bott, L.W. Tu, *Differential Forms in Algebraic Topology*, Springer New York, NY (1982), doi:[10.1007/978-1-4757-3951-0](https://doi.org/10.1007/978-1-4757-3951-0).
- [57] A. Hatcher, *Algebraic Topology*, Cambridge University Press, (2001), ISBN:9780521795401.
- [58] C. Devescovi, M. García-Díez, I. Robredo, M. Blanco de Paz, J. Lasa-Alonso, B. Bradlyn, J.L. Mañes, M.G. Vergniory, and A. García-Etxarri, *Cubic 3D Chern photonic insulators with orientable large Chern vectors*, Nat Commun **12**, 7330 (2021), doi:[10.1038/s41467-021-27168-w](https://doi.org/10.1038/s41467-021-27168-w).
- [59] K. Gomi, *Homological bulk-edge correspondence for Weyl semimetals*, Progress of Theoretical and Experimental Physics, **2022**, 4 04A106 (2022), doi:[10.1093/ptep/ptab035](https://doi.org/10.1093/ptep/ptab035).
- [60] G.-G. Liu, Z. Gao, Q. Wang, X. Xi, Y.-H. Hu, M. Wang, C. Liu, X. Lin, L. Deng, S.A. Yang, P. Zhou, Y. Yang, Y. Chong, and B. Zhang, *Topological Chern vectors in three-dimensional photonic crystals*, Nature **609**, 925–930 (2022), doi:[10.1038/s41586-022-05077-2](https://doi.org/10.1038/s41586-022-05077-2).

- [61] K. Gomi, *Twists on the Torus Equivariant under the 2-Dimensional Crystallographic Point Groups*, SIGMA **13**, 014 (2017), doi:[10.3842/SIGMA.2017.014](https://doi.org/10.3842/SIGMA.2017.014).
- [62] L.W. Tu, *Introductory Lectures on Equivariant Cohomology*, Princeton University Press (2020), doi:[10.2307/j.ctvrdflgz](https://doi.org/10.2307/j.ctvrdflgz).
- [63] D.H. Kobe, *Invariance of the generalised Berry phase under unitary transformations: application to the time-dependent generalised harmonic oscillator*, J. Phys. A: Math. Gen. **23** 4249, doi:[10.1088/0305-4470/23/19/012](https://doi.org/10.1088/0305-4470/23/19/012).
- [64] L. Michel, *Fundamental concepts for the study of crystal symmetry*, Physics Reports, **341**, 1–6 p. 265-336 (2001), doi:[10.1016/S0370-1573\(00\)00091-0](https://doi.org/10.1016/S0370-1573(00)00091-0).
- [65] E.J. Bergholtz, J.C. Budich, and F.K. Kunst, *Exceptional topology of non-Hermitian systems*, Rev. Mod. Phys. **93**, 015995 (2021), doi:[10.1103/RevModPhys.93.015005](https://doi.org/10.1103/RevModPhys.93.015005).
- [66] T. Kato, *Perturbation Theory for Linear Operators*, Springer-Verlag Berlin Heidelberg 1995, doi:[10.1007/978-3-642-66282-9](https://doi.org/10.1007/978-3-642-66282-9).
- [67] P. Delplace, T. Yoshida, and Y. Hatsugai, *Symmetry-Protected Multifold Exceptional Points and Their Topological Characterization*, Phys. Rev. Lett. **127**, 186602 (2021), doi:[10.1103/PhysRevLett.127.186602](https://doi.org/10.1103/PhysRevLett.127.186602).
- [68] W. Tang, K. Ding, and G. Ma, *Realization and topological properties of third-order exceptional lines embedded in exceptional surfaces*, Nat Commun **14**, 6660 (2023), doi:[10.1038/s41467-023-42414-z](https://doi.org/10.1038/s41467-023-42414-z).
- [69] T. Yoshida, J.L.K. König, L. Rødland, E.J. Bergholtz, M. Stålhammar, *Winding topology of multifold exceptional points*, Phys. Rev. Research **7**, L012021, (2025), doi:[10.1103/PhysRevResearch.7.L012021](https://doi.org/10.1103/PhysRevResearch.7.L012021).
- [70] M. Stålhammar, and L. Rødland, *Abelian spectral topology of multifold exceptional points*, Phys. Rev. Research **7**, 033246 (2025), doi:[0.1103/8lyx-vtnw](https://doi.org/10.1103/8lyx-vtnw).
- [71] D.F. Liu, A.J. Liang, E.K. Liu, Q.N. Xu, Y.W. Li, C. Chen, D. Pei, W.J. Shi, S.K. Mo, P. Dudin, T. Kim, C. Cacho, G. Li, Y. Sun, L. X. Yang, Z.K. Liu, S.S. P. Parkin, C. Felser, and Y.L. Chen, *Magnetic Weyl semimetal phase in a Kagomé crystal*, Science **365**, 6459 pp. 1282-1285 (2019), doi:[10.1126/science.aav2873](https://doi.org/10.1126/science.aav2873).
- [72] I. Belopolski et al., *Discovery of topological Weyl fermion lines and drumhead surface states in a room temperature magnet*, Science **365**, 6459 pp. 1278-1281, doi:[10.1126/science.aav2327](https://doi.org/10.1126/science.aav2327).
- [73] N. Morali, R. Batabyal, P.K. Nag, E. Liu, Q. Xu, Y. Sun, B. Yan, C. Felser, N. Avraham, and H. Beidenkopf, *Fermi-arc diversity on surface terminations of the magnetic Weyl semimetal  $\text{Co}_3\text{Sn}_2\text{S}_2$* , Science **365**, 6459 pp. 1286-1291, doi:[10.1126/science.aav2334](https://doi.org/10.1126/science.aav2334).
- [74] S. Peltier, S. Alayrangués, L. Fuchs, and J.-O. Lachaud, *Computation of Homology Groups and Generators*, Lecture Notes in Computer Science, **3429**, Springer, Berlin, Heidelberg (2005), doi:[10.1007/978-3-540-31965-8\\_19](https://doi.org/10.1007/978-3-540-31965-8_19).
- [75] A.M. Turner, Y. Zhang, R.S.K. Mong, and A. Vishwanath, *Quantized response and topology of magnetic insulators with inversion symmetry*, Phys. Rev. B **85**, 165120 (2012), doi:[10.1103/PhysRevB.85.165120](https://doi.org/10.1103/PhysRevB.85.165120).

- [76] M. Xiao, L. Ye, C. Qiu, H. He, Z. Liu, and S. Fan, *Experimental demonstration of acoustic semimetal with topologically charged nodal surface*, Sci. Adv. **6**, eaav2360 (2020), doi:[10.1126/sciadv.aav2360](https://doi.org/10.1126/sciadv.aav2360).
- [77] Q. Wang, Y. Ge, H.-X. Sun, H. Xue, D. Jia, Y.-J. Guan, S.-Q. Yuan, B. Zhang, and Y.D. Chong, *Vortex states in an acoustic Weyl crystal with a topological lattice defect*, Nat Commun **12**, 3654 (2021), doi:[10.1038/s41467-021-23963-7](https://doi.org/10.1038/s41467-021-23963-7).
- [78] K. Li, X. Zhang, Z. Zhang, Y. Cheng, and X. Liu, *Observation of chiral Landau levels in a synthetic acoustic Weyl semimetal*, Commun Phys **8**, 133 (2025), doi:[10.1038/s42005-025-02053-w](https://doi.org/10.1038/s42005-025-02053-w).
- [79] X.-Q. Sun, M. Xiao, T. Bzdušek, S.-C. Zhang, and S. Fan, *Three-Dimensional Chiral Lattice Fermion in Floquet Systems*, Phys. Rev. Lett. **121**, 196401 (2018), doi:[10.1103/PhysRevLett.121.196401](https://doi.org/10.1103/PhysRevLett.121.196401).
- [80] S. Higashikawa, M. Nakagawa, and M. Ueda, *Floquet Chiral Magnetic Effect*, Phys. Rev. Lett. **123**, 066403 (2019), doi:[10.1103/PhysRevLett.123.066403](https://doi.org/10.1103/PhysRevLett.123.066403).
- [81] Y. Zhu, T. Qin, X. Yang, G. Xianlong, and Z. Liang, *Floquet and anomalous Floquet Weyl semimetals*, Phys. Rev. Research **2**, 033045 (2020), doi:[10.1103/PhysRevResearch.2.033045](https://doi.org/10.1103/PhysRevResearch.2.033045).
- [82] T.E. O'Brien, C.W.J. Beenakker, and Ī. Adagideli, *Superconductivity Provides Access to the Chiral Magnetic Effect of an Unpaired Weyl Cone*, Phys. Rev. Lett. **118**, 207701 (2017), doi:[10.1103/PhysRevLett.118.207701](https://doi.org/10.1103/PhysRevLett.118.207701).
- [83] M. Stålhammar, D. Rudneva, T.H. Hansson, and F. Wilczek, *Emergent Chern-Simons interactions in 3+1 dimensions*, Phys. Rev. B **109**, 064514 (2024), doi:[10.1103/PhysRevB.109.064514](https://doi.org/10.1103/PhysRevB.109.064514).
- [84] J. Celeste, *Cohomology of knotted semimetals in three dimensions*, arXiv:2312.01667, doi:[10.48550/arXiv.2312.01667](https://doi.org/10.48550/arXiv.2312.01667).
- [85] J.L. Tu, *Twisted K-Theory and Poincaré Duality*, Transactions of the American Mathematical Society **361**, No. 3 pp. 1269-1278 (2009), doi:[10.48550/arXiv.math/0609556](https://doi.org/10.48550/arXiv.math/0609556).